CENTRIOLES FUNCTION AS SIGNALING CENTERS TO CONTROL PROLIFERATION IN CELLS WITH CENTRIOLE AMPLIFICATION

by
Lauren Taylor Evans

A dissertation submitted to Johns Hopkins University in conformity with the requirements for the degree of Doctor of Philosophy

Baltimore, Maryland
July 2021

Abstract

Centrioles are microtubule structures that form the two poles of the mitotic spindle and act as a structural scaffold upon which the primary cilium is built. To maintain the fidelity of these processes, centriole number is tightly regulated. When a cell possesses more than the canonical number of centrioles (4), a condition known as centriole amplification, it becomes susceptible to mitotic errors. Centriole amplification has been shown to promote spontaneous tumorigenesis *in vivo* and has been observed in a wide range of human tumors. Therefore, it was surprising to discover that centriole amplification induces a proliferative arrest in non-transformed cultured cells. A trimeric protein complex known as the PIDDosome has been shown to initiate a cell-cycle arrest in the presence of supernumerary centrioles. However, how a cell detects extra centrioles and relays this signal to the PIDDosome remains unknown.

To address this question, a genome-wide CRISPR/Cas9 knock-out screen was performed to identify genes required for the cell-cycle arrest following centriole amplification. We identified genes previously implicated in the response to extra centrioles, including all three components of the PIDDosome (PIDD1, CASP2, CRADD) as well as the downstream effectors P53 and P21. We also identified several novel regulators including ANKRD26, C2CD3 and SCLT1. Notably, these novel regulators are involved in the recruitment/formation of distal appendages, which are protein structures that decorate centrioles. Our data show that these structures also have a non-canonical role in triggering PIDDosome activation in response to centriole amplification.

In normal cells, there is only one centriole that contains distal appendage structures; therefore, our data support a model in which multiple centrioles with distal appendages is the signal by which a cell ‘senses’ centriole amplification. This work highlights a novel role of distal appendages in the response to centriole amplification and shifts the focus from centrioles as merely structural platforms required to build centrioles and cilia toward these organelles acting as signaling centers in mammalian cells.

Primary Reader and Advisor: Andrew Holland

Secondary Reader: Sergi Regot

Preface

This thesis would not have been possible if it were not for the tremendous amount of support I received from the people in my life. First and foremost, I would like to thank my mentor Andrew Holland for taking a chance on me and accepting me into his lab when I had little-to-no experience in Molecular and Cell Biology. Through your mentorship and your actions, you have always emphasized the importance of doing rigorous science and not being afraid to perform experiments that could call into question your model or hypothesis. You have had so much influence over the way I approach scientific questions and design experiments. I know I would not be the scientist I am today without you and the lessons I learned from you during my PhD will have an impact on me for the rest of my scientific career.

I also owe a lot of gratitude to the members of my lab who have offered me so much support and friendship over the years. To Bram, Michelle and Tyler, thank you for laying the foundation of the lab and building an environment where I immediately felt welcomed. You each acted as mentors for me throughout my graduate career and your continued support over the years has meant so much to me. Liz, thank you for being my first friend in the lab as well as my confidante and shoulder to cry on when the pressures of grad school were too much to handle. Phillip, your large personality and even larger heart have always helped pick me up whenever I was having a tough day. Coffee breaks will never be the same without you. And to all the other members of the Holland Lab who have made my time in graduate school so unforgettable, I thank you.

I would be remised if I did not acknowledge Thao, who has been my best friend and one of my biggest supporters during my PhD. I feel so fortunate that we have been able to experience the highs and the lows of grad school together. I never thought that when I came to Hopkins, I would meet someone who would have such a profound impact on my life the way you have. You are the yin to my yang and provide me with clarity I need when I am thinking irrationally. You have supported me throughout every step of this journey, and I know for a fact that I would not have made it through this PhD if it were not for you. I also know that our bond and this friendship will be something we share for the rest of our lives.

I would not be here today if it were not for my wonderful family, who have always supported by scientific journey, even if they did not understand what I was doing. To my parents, you were my first mentors and taught me how important it is to be curious and ask questions. You instilled in me a deep love of knowledge, which I apply to all of my scientific pursuits. I learned how to have a strong work ethic by watching you guys as you raised me and Jessica while each pursuing careers of your own. I would not have had the confidence or the ability to pursue this degree without your support or guidance. To my little sister, Jessica or as you will always be to me, Jessie, I have always strived to be the best that I can be in order to be a good role model for you. But over these last couple of years, you have been the one I look up to. Your resilience and success in your career are something I admire greatly, and I hope I can achieve these in my own career. I also want to thank all of the member of my extended family,

grandparents, aunts, uncles and many cousins, who have been supportive of me during this journey.

Last, but certainly not least, I would like to thank my boyfriend, Trevor. You have been my rock through this entire process. Every time I thought I couldn't do this, and I wanted to throw in the towel, you would reassure me and help me keep pushing forward. You have spent countless hours listening to my presentations and helping me edit my work, even though you have no clue what a centriole is. You are the kindest, most patient and smartest person I have every met and I am so grateful every day that you are a part of my life.

Contents

List of Tables

List of Figures

Chapter 1: Introduction

Centrosomes are the main microtubule organizing centers of mammalian cells and are composed of two orthogonally arranged microtubule structures called centrioles surrounded by a proteinaceous material called the pericentriolar material or PCM.[1,2] Centriole are involved in several cellular processes including organization of the microtubule network during interphase, formation of the bipolar spindle during mitosis and acting as a structural scaffold upon which the primary cilium is built. To ensure that these processes are carried out properly, centriole number is tightly controlled throughout the cell cycle[3] so that each pre-existing centriole undergoes only a single round of duplication, similar to the genetic material. Following mitosis, each daughter cell inherits a pair of centrioles. The two centrioles of this pair are structurally distinct from one another. One centriole is decorated with protein structures known as distal appendages and is referred to as the mature parent or mature mother centriole because it was built earlier than the immature parent centriole.[4] The immature parent centriole was built in the previous cell cycle and lacks appendages on its distal end. The immature centriole will eventually acquire distal appendages when it becomes mature during the G1 phase of the next cell cycle. These appendage structures are required to dock the centriole at the membrane during the process of ciliogenesis.[5] During the G1/S transition of the cell cycle, a new centriole begins to bud from the proximal end of each pre-existing centriole.[6] These new centrioles elongate throughout S-phase. During G2, the two original

centrioles separate from one another, producing two distinct centriole pairs or centrosomes. In mitosis, these structures become the two poles of the microtubule spindle which segregates chromosomes equally into the resulting daughter cells. Upon division the two centriole pairs are also partitioned into different daughter cells and the duplication process repeats.

Errors in the duplication process can result in extra centrioles or centriole loss.[1,7,8] Centriole loss is able to be tolerated in some species and cell populations, such as planarians or oocytes in humans.[9,10] During mitosis, centrioles play a role in microtubule nucleation and spindle assembly, however, spindle assembly can occur through centriole independent microtubule nucleation.[11] Although spindle assembly and chromosome segregation can occur in the absence of centrioles, mitoses in acentriolar cells are often result in segregation errors and aneuploidies.[12] In concert, cultured mammalian cells experience a P53-depedent growth arrest following centriole loss, indicating that centrioles are required to maintain faithful chromosome segregation and continued growth.

In acentriolar cells, spindle assembly and chromosome segregation is often delayed since cells must initiate microtubules nucleation by other means.[11] In the absence of centrioles, chromatin-dependent microtubule nucleation can compensate to help build the mitotic spindle.[13] Since chromatin is sequestered in the nucleus, it does not have access to microtubule dimers and, therefore, cannot begin nucleating microtubules until nuclear envelope breakdown (NEB). Microtubules can also be generated from spindle microtubules in a centriole-

independent manner[14]; however, this process requires a pre-existing microtubule scaffold. These factors contribute to the delay in spindle assembly in cells lacking centrioles.

Genome-wide knock-out screens were used to identify how cells lacking centrioles could activate a P53-dependant arrest. These screens led to the identification of a signaling pathways containing USP28, 53BP1, P53 and P21.[15–17] Knocking out any of these four genes allows cells with centriole loss to continue proliferating. Despite being required to arrest cells following centriole loss none of these proteins exhibit centriolar localization. This indicates that centriole loss itself is likely not the trigger that initiates the cell-cycle arrest in acentriolar cells. Once mitotic duration exceeds a particular threshold, cultured cells experience a subsequent G1 arrest.[15–17] Interestingly, all the genes identified as being required to arrest cells following centriole loss were also required for the growth arrest in cells with prolonged mitoses, regardless of whether centrioles were present or not.[15–17] Therefore, this pathway has been referred to as 'the mitotic surveillance pathway', since it appears to be sensing the extended mitotic time associated with centriole loss, rather than responding to changes in centriole number.

How the mitotic surveillance pathway is activated following prolonged mitosis remains unclear. It is known that 53BP1 interacts with P53 in response to DNA double-strand breaks[18] and that USP28 gets recruited to sites of DNA damage by 53BP1.[19] However, the role of these proteins in the mitotic surveillance pathway is known to be independent of the DNA damage response,

suggesting that additional regulators of this pathway remain to be identified. One could imagine that once the mitotic surveillance pathway is activated, 53BP1 acts as an adaptor to between the deubiquitinase USP28 and P53. USP28 may then deubiquitinate and stabilize P53, which elicits a P21 mediated cell-cycle arrest.

In addition to centriole loss, mitotic errors can result in an increase in centriole number. In cultured cells, the presence of supernumerary centrioles, a condition known as centriole amplification, is known to promote genetic instability through chromosome mis-segregation errors, chromosome breaks and DNA damage.[20] Centriole amplification has also been observed in a wide range of human tumors and often correlated with higher cancer grade and poor patient prognosis.[7] Additionally, centriole amplification has been proposed to promote metastasis via multiple mechanisms.[21,22] Centriole amplification has been modeled *in vivo* by overexpressing the dose-dependent master regulator of centriole biogenesis polo-like kinase 4 (PLK4).[23] In these models, the presence of supernumerary centrioles was shown to be sufficient to promote spontaneous tumorigenesis.[24–26]

Centriole amplification is also observed in tetraploid cells, which contain twice the normal number of centrioles (4 vs. 2 in G1).[21] Cells can become tetraploid by disrupting cytokinesis, which prevents daughter cells from separating from one another. Cytokinesis failure increases both the DNA content and centriole number in cells, whereas overexpression of PLK4 induces centriole amplification without a concurrent increase in genetic material. Like PLK4 overexpression, however, the increase in centriole number in tetraploid cells can

lead to mitotic errors and DNA damage. Only tetraploid cells that spontaneously lose their extra centrioles are able to continue proliferating in culture[27], highlighting the deleterious nature of centriole amplification. Additionally, tetraploidy induced through cytokinesis failure is able to promote tumorigenesis in P53-null cells.[28] This is consistent with the observation that whole-genome duplication (tetraplodization) occurs in ~30 % of solid tumors.[29]

Despite being found in a wide range of human tumors and being sufficient to promote tumorigenesis in animal models, centriole amplification leads to a cell cycle arrest in non-transformed cells in culture.[30,31] Loss of P53 is able to overcome the growth arrest observed in these cells with extra centrioles. This is consistent with the dysregulation of P53 observed in the tumors from *in vivo* models of centriole amplification.[24–26] These data indicate that the growth of cells with supernumerary centriole is disadvantageous and not tolerated in non-transformed cells.

Although the growth arrest following centriole loss and centriole amplification are both dependent on P53, USP28 and 53BP1 were found to be dispensable in response to extra centrioles.[15] This indicates that there are two distinct pathways operating in cells that respond to centriole number; one responsible for arresting cells with too few centrioles and one that arrests cells with extra centrioles.

Initial insight into how cells elicit a growth arrest following centriole amplification came from an siRNA screen performed in tetraploid cells containing twice canonical number of centrioles. This screen showed that the depletion of

the kinase LATS2 allowed tetraploid cells to overcome a G1 arrest. LATS2 is a component of the Hippo pathway, and was shown to facilitate P53 stabilization in the presence of supernumerary centrioles.[32] The Hippo tumor suppressor pathway plays a role in cell proliferation and cell death and is known primarily for regulating organ size.[33] The Hippo pathway controls cell growth through regulation of the transcriptional activators YAP/TAZ, which promote cell proliferation.[34] When the Hippo pathway is activated, YAP/TAZ are phosphorylated by the kinase LATS2, which sequesters them in the cytoplasm and prevents transcription of their pro-proliferative targets. Phosphorylated (active) LATS2 has also been shown to inhibit the E3-ubiquitin ligase MDM2, which stabilizes P53.

Tetraploid cells showed an increase in phosphorylated LATS2 and depletion of LATS2 in tetraploid cells was sufficient to overcome arrest.[32] In tetraploid cells, the LATS2-dependent arrest appeared to be reliant on both its ability to inactivate YAP/TAZ and through stabilization of P53. It was shown that the activation of the Hippo pathway in response to centriole amplification was dependent on reduced RhoA activity rather than MST1/MST2, which are canonically known to function upstream of LATS2.[32] This work implies a mechanism in which the presence of extra centrioles reduces RhoA activity, thus activating the Hippo pathway and inhibiting cell growth.

In addition to the Hippo pathway, other pathways have been implicated in the response to centriole amplification. It has been shown that the PIDDosome becomes activated in cells with extra centrioles.[30] The PIDDosome is a trimeric

protein complex composed of PIDD1, CRADD and Caspase-2 (CASP2).[35] PIDD1 and CRADD act as an activation platform for CASP2 by recruiting several inactive pro-CASP2 molecules so they can undergo proximity induced cleavage and activation.[35,36] Once activated, CASP2 cleaves MDM2 and stabilizes P53, which initiates a proliferative arrest.

CASP2 activation and MDM2 cleavage were both observed in cells that underwent cytokinesis failure.[30] Furthermore, loss of PIDD1, CRADD or CASP2 prevented MDM2 cleavage, indicating that this response was PIDDosome dependent. Inducing cytokinesis failure in cells lacking centrioles did not trigger activation of PIDDosome, indicating that this response is detecting the centriole amplification present in tetraploid cells rather than the increase in DNA content. Notably, activation of the PIDDosome was not observed by increasing mitotic duration or by inducing DNA damage. It was also shown that the core component of the PIDDosome, PIDD1, localizes to the mature mother centriole.[30] This suggests that it may be the presence of extra mature mother centrioles that elicits PIDDosome activation in cells with centriole amplification, however how this could occur is not known.

It is unclear whether the Hippo pathway or activation of the PIDDosome is predominantly responsible for arresting cells following centriole amplification or if these pathways work in concert to induce an arrest. Although activation of both the Hippo and PIDDosome pathways explain how P53 becomes stabilized following centriole amplification, it is still uncertain how the presence of extra

centrioles leads to such activation and if inactivation of these responses is sufficient to improve the long-term fitness of cells with centriole amplification.

To address these questions, we performed a genome-wide CRISPR/Cas9 knock-out screen to identify regulators of the response to centriole amplification in an unbiased way. The main goal of this work was to gain greater mechanistic insight into how cells ‘sense’ and respond to centriole amplification. Additionally, we sought to understand how cells could overcome this response and initiate tumorigenesis.

Chapter 2: Identification of novel regulators required to arrest cells following centriole amplification

2.1 Introduction

Centriole amplification makes a cell susceptible to genetic instability.[37] Additionally, the continued growth of cells with extra centrioles has been shown to promote spontaneous tumorigenesis *in vivo*.[24–26] To avoid propagation of genetically unstable cells, centriole amplification leads to a proliferative arrest in non-transformed, cultured cells. There have been several mechanisms proposed for how cells elicit a cell cycle arrest in the presence of extra centrioles, namely through the activation of the Hippo pathway or activation of the PIDDosome.[30,32]

It has been shown that tetraploid cells containing twice the normal number of centrioles, stabilize P53 via activation of the Hippo pathway.[32] The Hippo tumor suppressor pathway regulates cell proliferation primarily to control organ size during development. The Hippo pathway kinase LATS2 is activated in tetraploid cells. This activation leads to an inhibition of the YAP/TAZ transcriptional regulators, P53 stabilization and a proliferative arrest. LATS2 activation was also observed when centriole amplification was induced by over-expressing PLK4. These data indicate that centriole amplification may be initiating a cell-cycle arrest through activation of the Hippo pathway.

The PIDDosome has also been shown to be activated in response to centriole amplification in tetraploid cells.[30] The PIDDosome is a protein complex

responsible for activation of Caspase-2 (CASP2). This in turn leads to MDM2 cleavage, P53 stabilization and expression of the cyclin-dependent kinase inhibitor, P21. This response was also shown to be centriole, rather than ploidy, dependent, providing another mechanism for the cell-cycle arrest following centriole amplification.

Both of these proposed mechanisms involve P53 stabilization upon centriole amplification; however, it is not clear whether they work in concert to prevent proliferation or, if not, which is the predominant pathway operating in cells. Additionally, the upstream regulators that activate these pathways in response to centriole amplification remain unclear. In order to identify genes required for the proliferative arrest in cells with extra centrioles, we performed a genome-wide CRISPR/Cas9 knock-out screen.

2.2 Methods

2.2.1 CRISPR/Cas9 Genome-wide Knock-out Screen

CRISPR/Cas9 pooled, knockout screens were performed essentially as described.[15,38,39] RPE1 PLK4^{Dox} cells were infected with a lentivirus containing an sgRNA targeting TRIM37 or USP28. The sgRNA sequence targeting TRIM37 was CTCTAATTTAAATAGCATGG. The sgRNA sequence targeting USP28 was ATCAACTCTCCTCCAGTCAT. Infected cells were then selected with 400 µg/mL zeocin for 3 weeks and monoclonal knockout lines isolated and validated by immunoblotting.

The human Brunello CRISPR knockout sgRNA library was purchased from Addgene (a gift of David Root and John Doench; #73178) and plasmid DNA amplified according to the manufacturer's instructions. To produce virus, the Brunello pooled plasmid library and the lentiviral packaging plasmids psPAX2 and pMD2.G were co-transfected into 40 x 15 cm culture dishes of HEK293FT cells. 6 x 10^6 HEK293FT cells were seeded into a poly-l-Lysine-coated 15 cm culture dish the day before transfection. For each 15 cm dish, the following DNA was diluted in 1.2 mL OptiMEM (Thermo Fisher Scientific): 9 µg lentiviral vector, 12 µg psPAX2, and 3 µg pMD2.G. Separately, 70 µL of 1 µg/µL 25-kD polyethylenimine (Sigma-Aldrich) was diluted into 1.2 mL OptiMEM and incubated at room temperature for 5 min. After incubation, the DNA and polyethylenimine mixtures were combined and incubated at room temperature for 20 min. During this incubation, the culture media was replaced with 16 mL prewarmed DMEM + 1 % FBS. The transfection mixture was then added dropwise to the 15 cm dish. Viral particles were harvested at 24, 48 and 72 hr after the media change. Media collected from 24, 48 and 72 hr was pooled and filtered through a 0.45 µm PVDF syringe filter. The media was then concentrated using Amicon Ultra-15 Centrifugal Filter Unit with Ultracel-50 membrane (EMD Millipore Corporation cat# UFC905024). The virus was then frozen and stored at -80 ºC.

Cells were transduced with the Brunello library via spinfection as previously described.[15] To find the optimal virus volumes for achieving an MOI ~ 0.1, each new batch of virus was titered by spinfecting 3 x 10^6 cells with several

different volumes of virus. Briefly, 3 x 10^6 cells per well were seeded into a 12 well plate in growth media supplemented with 10 µg/mL polybrene. Each well received a different titrated virus amount (between 5 and 50 µL) along with a no-transduction control. The plate was centrifuged at 2,000 rpm for 2 hr at room temperature. After the spin, media was aspirated, and fresh growth media was added. The following day, cells were counted, and each well was split into duplicate wells. One well received 3 µg/mL puromycin (Sigma) for 3 days. Cells were counted and the percent transduction calculated as the cell count from the replicate with puromycin divided by the cell count from the replicate without puromycin multiplied by 100. The virus volume yielding a MOI closest to 0.1 was chosen for large-scale transductions.

For the pooled screen, a total of 1 x 10^8 $PLK4^{Dox}$; $TRIM37^{-/-}$ or $PLK4^{Dox}$; $USP28^{-/-}$ cells were infected at MOI ~0.1 and selected with puromycin at 3 µg/mL for 3 days. MOI was calculated using a control well infected in parallel following the same procedure outlined above. Infected cells were expanded under puromycin selection for 5 days and then seeded into 80 x 15 cm dishes with 250,000 cells per dish. 40 of the dishes received media supplemented with 400 µg/mL of G418 to maintain selection for the Tet-ON mPLK4 transgene and the other 40 dishes received 1 µg/mL of doxycycline and 400 µg/mL of G418. Cells were allowed to grow for 21 days without further passaging before being harvested for DNA extraction.

Cell pellets were resuspended in lysis buffer containing 50 mM Tris, 50 mM EDTA, 1 % SDS, pH 8 and 30 µL of 20 mg/mL proteinase K and incubated

at 55 ºC overnight. The next day, 30 µL of 10 mg/mL RNase A was added, and the sample was inverted 25 times and incubated at 37 ºC for 30 min. Samples were cooled on ice before adding 2 mL of chilled 7.5 M ammonium acetate. Samples were then vortexed at high speed for 20 sec and centrifuged at >4000 g for 10 min. The supernatants were decanted into new 15 mL conical tubes and 6 mL of 100 % isopropanol was added. The tubes were inverted 50 times and centrifuged at >4000 g for 10 min. The supernatant was discarded and 6 mL of freshly prepared 70 % ethanol was added to each tube. The tubes were inverted 10 times and centrifuged at >4000 g for 1 min. The supernatant was discarded, and the pellet was air dried for 30 min. Finally, 200 µL of 1 X TE buffer was added, and the tube was incubated at 65 ºC for 1 hr. DNA concentration was measured using a Nanodrop.

The sgRNA library for each sample was amplified and prepared for Illumina sequencing using a two-step PCR procedure as previously described.[15] For the first PCR, a region containing the sgRNA cassette was amplified using primers specific to the sgRNA-expression vector:

lentiGuide-PCR-F:AATGGACTATCATATGCTTACCGTAACTTGAAAGTATTTCG

lentiGuide-PCR1-R:CTTTAGTTTGTATGTCTGTTGCTATTATGTCTACTATTCTT TCC

The thermocycling parameters for the first PCR were: 98 °C for 30 sec, 18-24 cycles of (98 °C for 1 sec, 62 °C for 5 sec, 72 °C for 35 sec), and 72 °C for 1 min. 1.5 µg of DNA was used in each PCR reaction. Assuming 6.6 pg of DNA per cell, ~100X representation of the Brunello library required ~53 µg of DNA per sample

(36 PCR reactions). The resulting amplicons for each sample were pooled, gel purified and used for amplification with barcoded second PCR primers. For each sample we performed 12 reactions.

Primers for the second PCR include both a variable length sequence to increase library complexity and an 8 bp barcode for multiplexing of different biological samples:

F2: AATGATACGGCGACCACCGAGATCTACACTCTTTCCCTACACGACGCTC TTCCGATCT(4-7 bp random nucleotides)(8 bp barcode)TCTTGTGGAAAGGAC GAAACACCG

R2: CAAGCAGAAGACGGCATACGAGATGTGACTGGAGTTCAGACGTGTGCT CTTCCGATCTTCTACTATTCTTTCCCCTGCACTGT

5 µl of the product from the first PCR reaction were used and the thermocycling parameters for the second PCR were: 98 °C for 30 s, 18-24 cycles of (98 °C for 1 sec, 70 °C for 5 sec, 72 °C for 35 sec). Second PCR products were pooled, gel purified and quantified using the Next Library Quantification Kit (NEB). Diluted libraries with 5 % PhiX were sequenced with MiSeq (Illumina).

Sequencing data were processed for sgRNA representation using custom scripts. Briefly, sequencing reads were first demultiplexed using the barcodes in the forward primer and then trimmed to leave only the 20 bp sgRNA sequences. The spacer sequences were then mapped to the spacers of the designed sgRNA library using Bowtie.[40] For mapping, a maximum of one mismatch was allowed in the 20 bp sgRNA sequence. Mapped sgRNA sequences were then quantified by

counting the total number of reads. The total numbers of reads for all sgRNAs in each sample were normalized.

The screen was performed two independent times for both PLK4^{Dox}, TRIM37$^{-/-}$ and PLK4^{Dox}, USP28$^{-/-}$ cells. We used the MaGeCK scoring algorithm (model-based analysis of genome-wide CRISPR-Cas9 knockout) to analyze and the rank the genes from the screens.[41] We noted that some of the hits from the MAGeCK analysis contained sgRNAs with very low representation.[42] Among these low count hits were many mitochondria and ATP production related genes that are likely selected for by the doxycycline treatment. We therefore excluded all genes that did not show a ≥ 0.005 % representation for at least two sgRNAs from the doxycycline treated population from any transduction of either the PLK4^{Dox}; TRIM37$^{-/-}$ or PLK4^{Dox}; USP28$^{-/-}$ cell lines. Genes with an FDR cutoff of ≤ 0.4 were taken forward for further validation.

2.2.2 Growth Assays

For competition growth assays, RPE1 PLK4^{Dox} cells constitutively expressing EGFP and non-fluorescent RPE1 cells were mixed at a 1:1 ratio and seeded into duplicate wells. One well from each pair was treated with doxycycline. After 5 days, each well was trypsinized and analyzed on a Guava easyCyte flow cytometer to determine the fraction of GFP positive cells. For each well, the fraction of GFP positive cells was divided by the GFP negative cells. The value obtained from the doxycycline treated well was then divided by that obtained in the untreated well to determine the fold change in GFP positive cells.

For long-term growth assays, RPE1 PLK4^{Dox} cells were seeded into duplicate wells and one well form each pair was treated with 1 µg/mL doxycycline. Cell number was counted every 2 days in triplicate using a LUNA-II automated cell counter.

For clonogenic growth assays, 1 x 103 RPE1 PLK4^{Dox} cells were seeded into duplicate 10 cm dishes. One dish was treated with 1 ug/mL doxycycline and the other was life untreated. After 10 days, cells were fixed in methanol for 20 min and stained with crystal violet dye for 20 min at room temperature. Plates were then washed with ddH_2O and dried overnight. Images were captured on a Syngene G:Box.

2.3 Results

2.3.1 Centrioles trigger a proliferate arrest in cells

To study the impact of centrosome amplification on cell proliferation, we used hTERT immortalized RPE1 cells that can be induced with doxycycline (dox) to overexpress PLK4 (hereafter referred to as PLK4^{Dox}). PLK4^{Dox} cells efficiently cluster extra centrosomes during mitosis and undergo a robust P53-dependent cell cycle arrest in response to PLK4-induced centrosome amplification.[31] To determine if the cell cycle arrest that occurs following PLK4 overexpression is due to centrosome amplification or an alternative function of PLK4, we created dox-inducible PLK4 cells with or without the centriole cartwheel protein SAS6. To allow for the continued proliferation of *SAS6*$^{-/-}$ cells lacking centrioles, we performed experiments in a TRIM37 knockout background.[16,17] TRIM37 loss

allows for the continued growth of acentriolar cells, which would otherwise arrest. While TRIM37-knockout RPE1 cells experienced a proliferative arrest after 4 days of PLK4 overexpression, knockout of SAS6 overcame this proliferative arrest (Figure 2.1). This suggests the growth arrest induced by PLK4 overexpression is due to centrosome amplification and not an alternative function of PLK4.

2.3.2 A CRISPR/Cas9 screen identifies genes required for a proliferative arrest following centriole amplification

To gain insight into how cells respond to extra centrosomes, we designed and executed a genome-wide CRISPR-Cas9 knockout screen to identify genes required to arrest proliferation following centrosome amplification. We utilized PLK4^{Dox} cells carrying a mouse PLK4 transgene that would not be targeted by the human PLK4 sgRNAs encoded in the sgRNA library. We also knocked out USP28 or TRIM37, which allows for cell proliferation following centrosome loss but not following centrosome amplification.[15–17] We anticipated two mechanisms by which PLK4-overexpressing, USP28 or TRIM37 knockout cells could be permitted to proliferate: 1) Loss of genes required for centriole duplication or stability, and 2) Loss of genes required to arrest the growth of cells with extra centrosomes (Figure 2.2).

Cas9-expressing PLK4^{Dox}; *USP28*$^{-/-}$ and PLK4^{Dox}; *TRIM37*$^{-/-}$ RPE1 cells were infected with a genome-wide sgRNA library containing 4 independent sgRNAs for every human gene (Figure 2.2). Transduced cells were selected for 7 days with puromycin, and knockout libraries of cells were treated with dox to

induce centrosome amplification and a subsequent cell cycle arrest. After three weeks of dox treatment, cells were harvested, and sgRNA abundance was analyzed. sgRNAs that provide a growth advantage were expected to be enriched in the dox treated population compared with untreated controls. The screen was repeated twice for both PLK4^{Dox}; *USP28*$^{-/-}$ and PLK4^{Dox}; *TRIM37*$^{-/-}$ cells, and the data from the four screens were analyzed together using the MAGeCK method for prioritizing genes and pathways[41] (Table 2.1, Figure 2.2).

Of the top 30 hits (FDR $\leq$ 0.4) identified in our screen, 23 were genes that encode proteins reported to localize to the centrosome (Table 2.2). From the top 30 hits of our screen, 14 genes had firmly established roles in centriole assembly/stability and were not analyzed further. sgRNAs targeting these genes were enriched in our screen because knocking-out these genes prevents centriole duplication and leads to centriole loss. TP53 and P21 were both present in the remaining 16 genes. Notably, all three components of the PIDDosome (PIDD1, CRADD and CASP2) were identified among the top hits from our screen, but LATS2 or any other component of the Hippo signaling pathway was not.

Cells expressing sgRNAs targeting each of the remaining 16 genes exhibited high levels of centrosome amplification following PLK4 overexpression, indicating that knockout of these genes didn't prevent centrosome amplification. We performed competition-based growth assays to validate that knockout of these genes enhanced the proliferation of PLK4^{Dox} cells with extra centrioles. As expected, sgRNAs targeting CRADD, PIDD1, CASP2, TP53 and P21 increased

cell proliferation in response to PLK4 overexpression (Figure 2.2). Furthermore, sgRNAs targeting 4 of the remaining 11 genes tested (FOPNL, C2CD3, SCLT1, and ANKRD26) increased the proliferation of cells with centrosome amplification more than three standard deviations above the mean of control cells. In summary, we identified all the known components of the PIDDosome pathway along with FOPNL, C2CD3, SCLT1, and ANKRD26 as playing a role in suppressing the proliferation of cells with extra centrosomes.

2.4 Discussion

Two distinct pathways have been proposed to restrict the proliferation of cells with centriole amplification. One is through the activation of the Hippo tumor suppressor pathway and the second is through activation of the PIDDosome. Both of these responses require P53 stabilization to elicit an arrest. However, the mechanism(s) through which these pathways become activated by extra centrioles remains poorly understood.

We show that PLK4 overexpression in an acceptable means of modeling centriole amplification. Utilizing CRISPR/Cas9 screening technology, we were able to identify genes that limit the proliferation of cells with extra centrosomes induced through PLK4 overexpression. All three components of the PIDDosome were identified as top hits in our screen, however, LATS2 or any other component of the Hippo pathway was not.

This does not necessarily mean that the Hippo pathway is not involved in responding to centriole amplification. LATS2 may not have been identified in out

screen for several reasons. First, activation of LATS2 in tetraploid cells may be due to an increase in DNA content rather than centriole amplification prese. In our screen centriole amplification was driven through overexpression of PLK4, which would increase centriole number without a concurrent increase in ploidy. Second, loss of LATS2 may only provide cells with a mild growth advantage in the presence of extra centrioles. If this is the case, then *LATS2*$^{-/-}$ may not have possessed the fitness required to compete in our screen and come out as a top hit. Lastly, knocking-out LATS2 may make cells generally unfit and unable to become enriched in our screen. Previous studies of the Hippo pathway in tetraploid cells utilized RNAi knock-down of LATS2[32], which may be better tolerated by cells. This is supported by the finding that complete disruption of the *Lats2* gene in mice results in embryonic lethality.[43]

Recent work from multiple labs, however, calls into question the involvement of the Hippo pathway in the response to supernumerary centrioles.[30,44,45] Loss of LATS2 was not able to overcome the growth arrest associated with centriole amplification induced through either cytokinesis failure[30] or PLK4 overexpression.[44] Additionally, the study that first suggested the Hippo pathways involvement in the response to extra centrioles was studying genes that, when knocked-down, allow cells to progress through G1 after tetraploization. This is not, necessarily a read-out of continued growth. It is possible that centriole amplification ultimately leads to an arrest in LATS2-defficient cells, just during a later cell-cycle.

In addition to the previously identified regulators of the response to supernumerary centrioles, we also identified four (4) additional genes (FOPNL, C2CD3, SCLT1 and ANKRD26) that may function as novel regulators. Cells which were knocked-out of each of these genes experienced robust centrosome amplification but did not cease proliferation in response. This indicates that they these novel regulators are playing a role in the cell-cycle arrest experienced in cells with extra centrioles.

2.5 Tables for Chapter 2

Table 2.1: Ranking of positively selected genes from MAGeCK analysis of the CRISPR/Cas9 knockout screen with FDR <1

Gene name	Score	P-value	FDR	Rank
C14orf80	1.49E-13	2.59E-07	0.000707	1
SASS6	2.73E-11	2.59E-07	0.000707	2
C16orf59	4.32E-10	2.59E-07	0.000707	3
TUBD1	1.11E-09	2.59E-07	0.000707	4
HYLS1	2.12E-08	2.59E-07	0.000707	5
STIL	2.80E-08	2.59E-07	0.000707	6
RTTN	5.43E-08	2.59E-07	0.000707	7
PPP1R35	1.32E-07	7.77E-07	0.001856	8
CEP120	3.84E-07	1.30E-06	0.00275	9
CRADD	1.22E-06	3.89E-06	0.006188	12
CENPJ	3.58E-06	1.48E-05	0.017636	16
PIDD1	6.34E-06	2.67E-05	0.028328	18
CASP2	1.13E-05	4.74E-05	0.038573	23
TUBE1	1.28E-05	5.41E-05	0.041386	25
PIBF1	1.92E-05	7.85E-05	0.048387	31
CDKN1A	2.61E-05	0.00010179	0.055587	35
FOPNL	2.72E-05	0.00010697	0.056793	36
EIF3H	5.02E-05	0.00018778	0.081571	44
TP53	6.19E-05	0.00022146	0.084653	50
C2CD3	0.0001139	0.00039189	0.12914	58
STT3B	0.00016719	0.00054988	0.163441	63
SPICE1	0.00025879	0.00079957	0.193445	79
CEP295	0.0006186	0.0017662	0.282715	119
SCLT1	0.000685	0.0019418	0.295042	125
ANKRD26	0.00084816	0.0023723	0.328208	137
CEP152	0.0012426	0.0034912	0.383596	173
NXT1	0.0014144	0.0039416	0.394459	190
KIAA0753	0.0014905	0.0041584	0.395305	196
CEP350	0.0016235	0.0045211	0.397544	217
CEP44	0.002158	0.0059446	0.417468	267
ZCCHC14	0.0022678	0.0062554	0.419343	283
SCAP	0.0052097	0.011918	0.53978	422

SIGLEC7	0.0061099	0.013485	0.562136	454
WBP11	0.011553	0.023021	0.694014	634
BRD9	0.018535	0.034855	0.779162	855
UBE2C	0.022183	0.041088	0.811193	966
CTSE	0.024959	0.04574	0.833387	1049
C12orf49	0.026166	0.047762	0.837492	1090
PHF6	0.028021	0.050892	0.848785	1146
BARHL1	0.030989	0.05585	0.861302	1239
TUSC5	0.036663	0.065209	0.872086	1419
MAGEE2	0.03763	0.066802	0.873522	1460
TRIM65	0.040474	0.071558	0.888109	1540
OFD1	0.042646	0.075161	0.896163	1603
NIPAL3	0.042763	0.075373	0.89723	1605
NGFRAP1	0.042891	0.075579	0.89723	1610
PHIP	0.043607	0.076736	0.897968	1632
MED25	0.044044	0.0775	0.899533	1646
SHROOM2	0.049522	0.081917	0.9135	1713
LGALSL	0.053747	0.085185	0.927651	1755
PPP1R8	0.057356	0.087989	0.934293	1800
KRTAP9-2	0.058157	0.088619	0.936824	1808
CYSTM1	0.068916	0.097052	0.965117	1922
ACKR2	0.070998	0.09868	0.970447	1943
KDELC2	0.071889	0.099387	0.971652	1955
SRI	0.074113	0.10115	0.976865	1979
CHD8	0.075397	0.10219	0.978615	1995
ZC2HC1B	0.077418	0.1038	0.979995	2024
GJC2	0.082776	0.10804	0.985269	2095
ZDHHC15	0.083756	0.10881	0.98695	2107
CCL1	0.083903	0.10894	0.987275	2109
NIPA1	0.085764	0.11042	0.989869	2132

Table 2.2: Protein function and localization of the Top30 hits from the CRISPR/Cas9 screens

Rank	Gene	Classification	Localization	Reference
1	TEDC1	Centriole assembly	Centriole	Breslow et al., 2018
2	SASS6	Centriole assembly	Centriole	Leidel et al., 2005
3	TEDC2	Centriole assembly	Centriole	Breslow et al., 2018
4	TUBD1	Centriole assembly	Centriole	Wang et al., 2017
5	HYLS1	Cilia assembly	Centriole	Dammerman et al., 2009; Hou et al., 2020
6	STIL	Centriole assembly	Centriole	Vulprecht et al. 2012; Arquint C, 2012, Tang et al., 2011
7	RTTN	Centriole assembly	Centriole	Chen et al, 2017
8	PPP1R35	Centriole assembly	Centriole	Fong et al. 2018; Sydor et al. 2018
9	CEP120	Centriole assembly	Centriole	Mahjoub et al., 2010
10	CRADD	Centriole amplification response	Cytoplasm	Fava et al., 2017
11	CENPJ	Centriole assembly	Centriole	Tang et al., 2009
12	PIDD1	Centriole amplification response	Centriole distal appendage	Fava et al., 2017
13	CASP2	Centriole amplification response	Cytoplasm	Fava et al., 2017
14	TUBE1	Centriole assembly	Centriole	Wang et al., 2017
15	PIBF1 (CEP90)	Cilia assembly	Centriole satellites	Kim et al., 2012
16	P21 (CDKN1A)	Centriole amplification response	Cytoplasm	Holland et al., 2012
17	FOPNL (FOR20)	Cilia assembly	Centriole satellites	Sedjaï et al., 2010
18	EIF3H	Translation initiation	Cytoplasm	
19	TP53	Centriole amplification response	Nuclear	Holland et al., 2012
20	C2CD3	Centriole amplification response	Centriole distal appendage	This study

21	STT3B	Post translational modification	Endoplasmic reticulum	
22	CEP135	Centriole assembly	Centriole	Yu-Chih et al., 2013
23	SPICE1	Centriole assembly	Centriole	Archinti et al., 2010
24	CEP295	Centriole assembly	Centriole	Izquierdo et al., 2014
25	SCLT1	Centriole amplification response	Centriole distal appendage	This study
26	ANKRD26	Centriole amplification response	Centriole distal appendage	This study
27	CEP152	Centriole assembly	Centriole	Hatch et al., 2010, Cizmecioglu et al., 2010
28	NXT1	Nuclear export	Nuclear	
29	KIAA0753	Cilia assembly	Centriole satellites	Chevrier et al., 2016
30	CEP350 (CAP350)	Cilia assembly	Centriole	Mojarad et al., 2017

2.6 Figures for Chapter 2

Figure 2.1

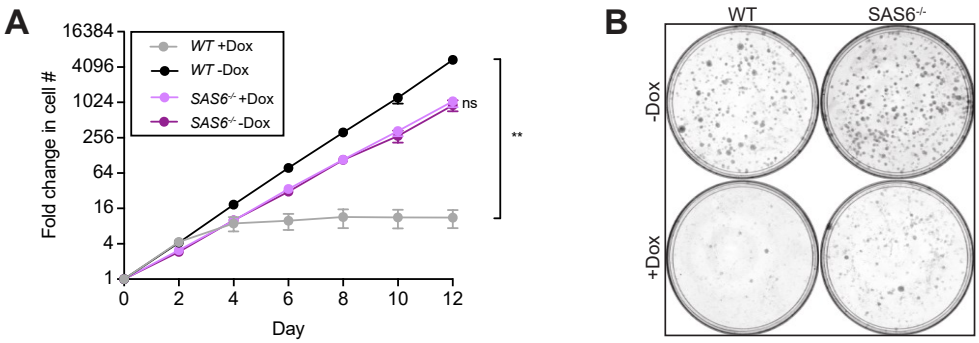

Figure 2.1: PLK4-induced centriole amplification is required for a cell-cycle arrest. **A.** Growth assay of the indicated cells with and without doxycycline-inducible overexpression of PLK4. Experiments were performed in wild-type or SAS6 monoclonal knockout cells. Data acquired across n = 3 biological replicates. Mean ± s.e.m. **B.** Clonogenic growth assay images of the indicated cells with and without doxycycline-inducible overexpression of PLK4.

Figure 2.2

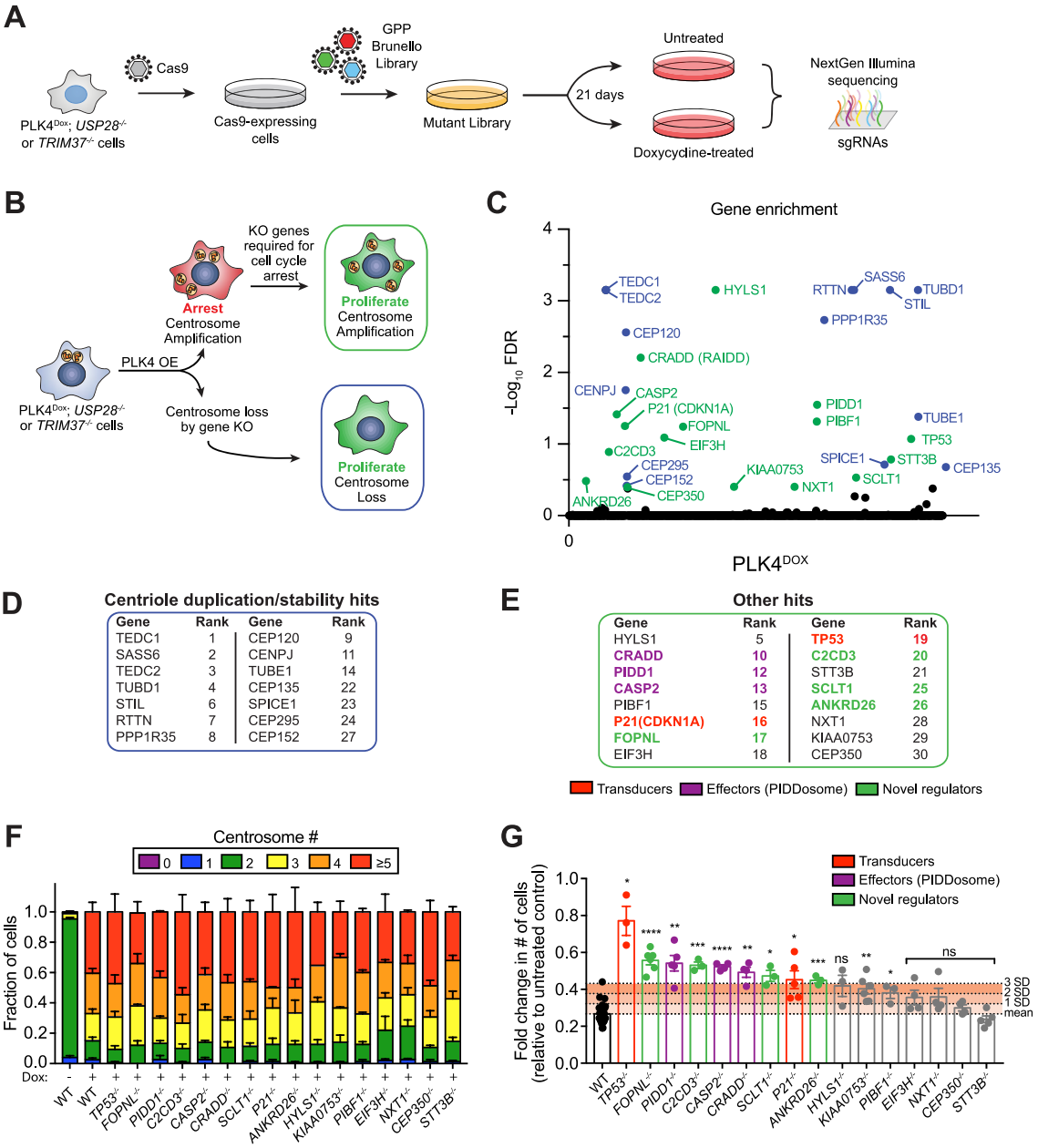

Gene	Rank	Gene	Rank
TEDC1	1	CEP120	9
SASS6	2	CENPJ	11
TEDC2	3	TUBE1	14
TUBD1	4	CEP135	22
STIL	6	SPICE1	23
RTTN	7	CEP295	24
PPP1R35	8	CEP152	27

Gene	Rank	Gene	Rank
HYLS1	5	TP53	19
CRADD	10	C2CD3	20
PIDD1	12	STT3B	21
CASP2	13	SCLT1	25
PIBF1	15	ANKRD26	26
P21(CDKN1A)	16	NXT1	28
FOPNL	17	KIAA0753	29
EIF3H	18	CEP350	30

Figure 2.2: A genome-wide CRISPR/Cas9 knockout screen identifies regulators of the response to centriole amplification. **A.** Schematic showing the procedure for a CRISPR/Cas9 positive selection screen to identify gene knockouts that increase the proliferation of cells with extra centrosomes. **B.** Schematic overview of the screen design. **C.** Top hits that emerged from the screens ranked by MaGeCK FDR value. Blue hits are genes required for centriole duplication or stability. Green hits are genes predicted to be required to arrest the growth of cells with extra centrosomes. **D.** Hits with known role in centriole duplication or stability. **E.** Candidate hits responsible for arresting the proliferation of cells with centrosome amplification. Purple hits correspond to PIDDosome genes. Red hits correspond to downstream effectors. Green hits are novel regulators. **F.** Quantification of centrosome number in PLK4Dox cells expressing an sgRNA targeting the indicated genes. Experiments were performed in polyclonal knockout cells. **G.** Graph showing the relative growth of doxycycline treated PLK4Dox cells expressing an sgRNA targeting the indicated genes. Each dot displays measurements from a single experiment. Experiments were performed in polyclonal knockout cells. Data acquired across n ≥ 3 biological replicates. Mean ± s.e.m. Data acquired across n ≥ 3 biological replicates. Mean ± s.e.m. Data information: Asterisks indicate statistically significant differences between measurements (*: P<0.05; **: P<0.01; ***: P<0.001, ****: P<0.0001). Statistics for all Figures were calculated using a two-tailed Student's t-test.

Chapter 3: Centriole distal appendages are required for the growth arrest in cells following centriole amplification

3.1 Introduction

Following mitosis, a cell inherits two centrioles which differ from one another in both age and structure.[1] One of the centrioles was just built in the previous cell-cycle and is, therefore, “younger” than the other centriole which was built earlier. The older centriole, referred to as the mature parent or mature mother centriole, is decorated with protein structures called distal appendages, while the younger centriole lacks such structures.

In quiescent cells, the centriole acts as a basal body, which docks at the plasma membrane and forms the structural scaffold upon which the primary cilium is built. During this process distal appendages on the mature mother centriole are important for the membrane docking process and ciliogenesis.[5] Distal appendages may also play a role in cilia gating, selectively allowing proteins to enter and exit the ciliary compartment.[46] Cilia are necessary for proper development and defects in these structures lead to a large range of disease, known as ciliopathies.[47] The distinction between the mature mother centriole with distal appendages and the immature centriole without appendages is required to ensure that only a single primary cilium is built.

In normal cycling cells, there is only ever one mature mother centriole that contains distal appendage structures[6], however these structures are dispensable

for cell division.[48] During mitosis the distal appendages undergo remodeling and the outer-most components are temporarily lost.[49] Appendages are then fully re-assembled during G1 of the following cell cycle on the more mature centriole. It takes 1.5 cell cycles before a centriole is capable of acquiring distal appendages and receiving the title of mature mother.[6]

Interestingly, the core component of the PIDDosome, PIDD1, has been shown to localize to the mature mother centriole.[30] Knock-out of appendage protein ODF2 impaired distal appendage assembly and PIDD1 localization to the centriole, indicating that appendages are required for PIDD1 recruitment. Furthermore, in cells lacking distal appendages, PIDDosome activation was not observed following centriole amplification.[30] These data show that PIDD1 localization to the mature mother centriole is essential for the response to supernumerary centrioles.

We identified nine genes form our CRISPR/Cas9 knock-out screen required to prevent proliferation in cells with centriole amplification. Five of these genes were previously shown to be involved in arresting cells with extra centrioles (P53, CASP2, CRADD, PIDD1 and P21). The remaining four genes (FOPNL, C2CD3, SCLT1 and ANKRD26) are novel regulators whose involvement in initiating an arrest remains to be discovered. Intriguingly, all four of these genes are related to distal appendage formation or cilia assembly. FOPNL encodes a protein required for cilia formation; C2CD3, encodes a protein required for distal appendage assembly;[50] and SCLT1 and ANKRD26 encode distal appendage proteins.[5,49,51] This suggests that centriole distal appendages

may function in responding to centriole amplification. We set out to test this hypothesis.

3.2 Methods

3.2.1 Stochastic optical reconstruction microscopy (STORM)

3.2.1a Immunofluorescence for STORM

Cells were grown on 25 mm, 1.5 high tolerance coverslips (Warner Instruments). Cells were fixed in 1.5 % formaldehyde for 4 min then permeabilized in 0.05% Triton for 30 sec. Samples were washed in 1X PBS and blocked in IF buffer (1% BSA, 0.05 % Tween-20, in 1 X PBS) for 15 min. Cells were incubated with primary antibody diluted in IF buffer at 37 °C for 3 hr. After washing in 1X PBS, cells were incubated with secondary antibody diluted IF buffer at 37 °C for 3 hr. The following primary antibodies were used: CEP164 (rabbit, recognizing aa: 1–112, Proteintech, 22227-1-AP, 1:3500), PIDD1 (mouse, Enzo, ALX-804837C100, 1:500). Conjugated secondary antibodies CF647 anti-mouse (Biotium, 20042) and CF568 anti-rabbit (Biotium, 20099) were used at 1:800 dilution.

3.2.1b STORM imaging

Samples were layered with 100 nm tetra-spectral fluorescent spheres (Invitrogen), which served as fiducial markers. Coverslips were mounted in Attofluor Cell chambers (Thermofisher) in imaging buffer (25 mM β-mercaptoethylamine, 0.5 mg/mL glucose oxidase, 67 µg/mL catalase, 10 % dextrose, in 100 mM Tris at pH 8.0). 3D STORM imaging was performed on a

Nikon N-STORM4.0 system using an Eclipse Ti inverted microscope, Apo TIRF 100X SA NA 1.49 Plan Apo oil objective, 405, 561,488 and 647 nm excitation laser launch and a back-illuminated EMCCD camera (Andor, DU897). The 647 nm laser line (~150 mW out of the fiber and ~90 mW before the objective lens) was used to promote fluorophore blinking. The 405 nm laser was used to reactivate fluorophores. The 561 nm laser was used to record the signals of fiducial markers. 20,000 to 30,000-time points were acquired at a 50 Hz frame rate each 16-20 ms. NIS Elements (Nikon) was used to analyze the data. Prior to STORM imaging, the position of CEP164 and PIDD1 was recorded in wide-field mode. The original storm Z color coding scheme illustrating the calibrated Z range (from red for the signals closer to the coverslip to blue for the signals further from the coverslip) is preserved on STORM images, which are presented as a projection of the entire 3D volume. The outer and inner diameters of distal appendage proteins were determined by measuring the diameters of the circles outlining the outer and inner edges of the STORM signal.[49]

3.2.2 Fluorescent recovery after photo-bleaching (FRAP)

To create the DLD1; PIDD1-2xmNeonGreen cell line, an sgRNA targeting the PIDD1 gene (5′-cccagagcctgcccaggcct-3′) was cloned into a pX459 vector (#62988; Addgene). To generate the PIDD1 repair vector, we cloned a 2× mNeonGreen tag followed by a T2A-neomycin and a translational stop codon into a modified pUC vector. 500 bp 5′ and 500 bp 3′ homology arms were PCR amplified from genomic DLD1 DNA and cloned on either side of the central 2′ mNeonGreen-T2A-Neomycin cassette. DLD1 cells were transiently transfected

(X-tremeGENE HP, Roche) with the pX459 plasmid and repair vector. Selection of transfected cells was performed 5 days after transfection with 400 µg/ml G418.

DLD1 PIDD1-AausFP1 (PIDD1 overexpressing cells) were generated by FLP-IN. PIDD1-AausFP1 was cloned into a pcDNA5 vector and then transfected into DLD1 LacZeo cells along with the pOG44 FLP recombinase expression vector using XtremeGene HP. Cells were selected with Hygromycin for 14 days. Colonies that grew out were pooled together. Cells were treated with doxycycline for 48 hrs prior to analysis.

FRAP was performed using a Lecia SP8 confocal microscope. Three images were collected prior to bleaching. A 3 µm region encompassing the PIDD1 foci was bleached with 80% laser intensity and then mages were then taken every 10 or 30 sec for 5 or 15 min to measure recovery.

3.3 Results

3.3.1 PIDD1 localizes to centriole distal appendages

PIDD1 has been reported to decorate mature centrioles.[30] An antibody raised against a PIDD1 death domain showed numerous cytoplasmic foci in addition to a signal that co-localized with the distal appendage of mature parent centrioles. The centriole staining of PIDD1 was lost in *PIDD1*$^{-/-}$ RPE1 cells while the cytosolic foci persisted, suggesting that the cytoplasmic staining is likely to be non-specific (Figure 3.1). Consistent with this interpretation, endogenously tagged PIDD1-2XmNeonGreen showed a highly specific localization at the centriole distal appendage in DLD1 cells and did not label cytosolic structures.

Importantly, PIDD1 was observed to localize to the mature mother centriole in both cells with normal and amplified centrosome numbers. 3D STORM was performed to characterize PIDD1 centriolar localization. This revealed that PIDD1 exhibited a nine-fold localization pattern around the top of the centriole, consistent with that of distal appendage proteins. PIDD1 had an inner and outer diameter of ~349 and ~595 nm, respectively, and its localization was most similar to that of ANKRD26,[49] which has previously been shown to localize at the outer portion of the distal appendage and was also a hit in our screen.

3.3.2 Centriole distal appendages are required for PIDD1 recruitment and the cell-cycle arrest in cells with extra centrioles

We tested whether sgRNAs targeting each of the 9 genes that function to suppress the growth of cells with extra centrosomes disrupted the centriole recruitment of PIDD1 (Figure 3.2). sgRNA-mediated disruption of CRADD, CASP2, TP53, and P21 did not affect the centriole localization of PIDD1. By contrast, sgRNAs targeting the novel regulators FOPNL, C2CD3, SCLT1 or ANKRD26, dramatically reduced the fraction of cells that recruited PIDD1 to the centriole. As mentioned previously, all four of these proteins play a role in distal appendage or cilia assembly.

Previous work has established a hierarchy for centriole distal appendage assembly in which C2CD3 is required to recruit CEP83, which recruits SCLT1 and finally ANKRD26 (Figure 3.2).[5,49] C2CD3, SCLT1, and ANKRD26 were identified in the top 30 hits of our screens, while CEP83 did not score highly. To

examine the role of all of these genes, we established monoclonal PLK4^{Dox} knockout cell lines for C2CD3, ANKRD26, SCLT1, and CEP83. Knockout of all four genes improved cell proliferation following centrosome amplification (Figure 3.2) and almost completely abolished the recruitment of PIDD1 to the mature parent centriole. These data show that distal appendages are required to recruit PIDD1 to mature centrioles and to inhibit cell growth in response to centrosome amplification.

3.3.3 PIDD1 does not dynamically turn over at the centriole

PIDD1 localizes to the mature mother centriole irrespective of centriole amplification, therefore recruitment to the centriole alone is not sufficient to promote PIDDosome activation. We envisioned that PIDD1 may be stably bound to distal appendages in cells with normal centriole number, but in cells with extra centrioles it might become processed at the centriole and released into the cytosol to form an active PIDDosome.

To investigate if PIDD1 dynamics at the centriole change upon centriole amplification, fluorescence recovery after photo-bleaching (FRAP) was performed on the centriolar pool of PIDD1 in DLD1 *PIDD1*-2XmNeonGreen endogenously tagged cells. No PIDD1 turnover was observed, regardless of centriole number (Figure 3.3), indicating that PIDD1 release is not a likely mechanism of PIDDosome activation. This experiment was repeated DLD1 cells overexpressing a fluorescently tagged PIDD1 cDNA. In these cells, moderate PIDD1 turnover was observed, suggesting that PIDD1 only turns over at the

centriole when overexpressed to non-physiological levels. This may explain why the centriolar pool of PIDD1 was previously reported to exhibit high turnover.[45]

3.4 Discussion

Centriole distal appendages are known to function in basal body docking at the centriole during the process of ciliogenesis in quiescent cells[5], however the role that distal appendages play in cycling cells remains unclear. It is largely believed that distal appendages are unnecessary in cycling cells, since these structures are not required for successful cell division.[48]

The requirement of centriole distal appendages for PIDDosome activation following centrosome amplification suggests that these structures are essential for initiating the proliferative arrest and are being actively monitored in cells. This is consistent with a previously model in which an increase in the number of mature parent centrioles was proposed to be the cue that triggers PIDDosome activation.[30] We show that PIDD1 localizes to that distal appendages in cells with normal centriole number as well as in cells with centriole amplification. This raises the question, how does the PIDDosome become specifically activated in cells with supernumerary mature mother centrioles?

Based on our FRAP data, it is evident that PIDD1 is not being processed at the centriole and released into the cytosol to form an active PIDDosome. It is possible, however, that cells with extra mature mother centrioles cluster these structures in order to; 1.) increase the local PIDD1 concentration enough to reach and activation threshold, 2.) arrange PIDD1 molecules in the correct orientation

to form an active PIDDosome complex, or 3.) facilitate a conformational change in PIDD1 which leads to its activation. Consistent with this idea, supernumerary centrioles have been shown to cluster in both interphase and mitotic cells[21], and PIDD1 in these centrioles clusters are arrange in close proximity to one another.[45]

The active PIDDosome complex has been shown to be composed of five PIDD1 and seven CRADD proteins, which interact with each other via their death domains.[52] We illustrate that PIDD1 interacts with the distal appendages and that its localization at the mature mother centriole exhibits a 9-fold symmetrical pattern. In support of the clustering model, it is unlikely that at a single centriole PIDD1 would be able to attain the conformation required to form an active PIDDosome.

3.5 Figures for Chapter 3

Figure 3.1

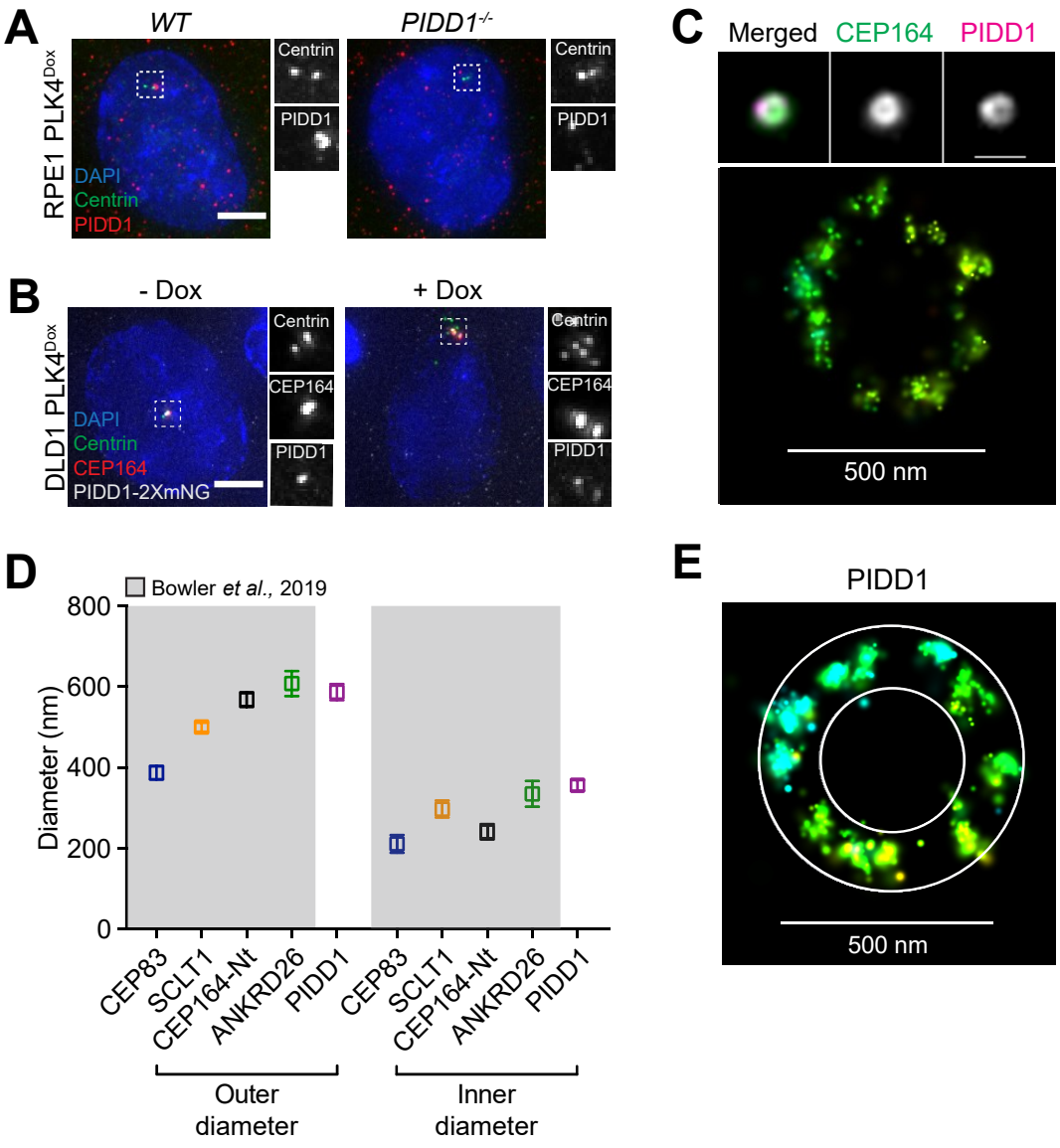

Figure 3.1: PIDD1 localizes to the distal appendages of the mature mother centriole. **A.** Representative images of wild-type and *PIDD1*$^{-/-}$ PLK4^{Dox} RPE1 cells immunostained with the indicated antibodies. Scale bar = 5 μm. **B.** Representative images of PLK4^{Dox} *PIDD1*-mNeonGreen DLD1 cells treated with and without doxycycline for 2 days and immunostained with the indicated antibodies. Scale bar = 5 μm. **C.** Top, widefield image showing the localization of CEP164 and PIDD1 at the mature- mother centriole. Bottom: Representative 3D STORM image of the same centriole showing PIDD1 localization. STORM image colors correspond to the Z-depth with red being the closest to the coverslip and blue being the most distant. **D.** Inner and outer diameter measurements for distal appendage proteins and PIDD1. Measurements in the shaded region were previously reported in (Bowler et al., 2019). Data displayed as box and whisker plots, where the box represents the upper and lower quartile and the whiskers represent the s.d. Scale bars: 1 μm for all wide-field images of centrioles and 500 nm for STORM images. Data acquired across n ≥6 cells. **E.** 3D STORM image of PIDD1 at the mature mother centriole. The overlaid mask represents the inner and outer diameters of the PIDD1 signal.

Figure 3.2

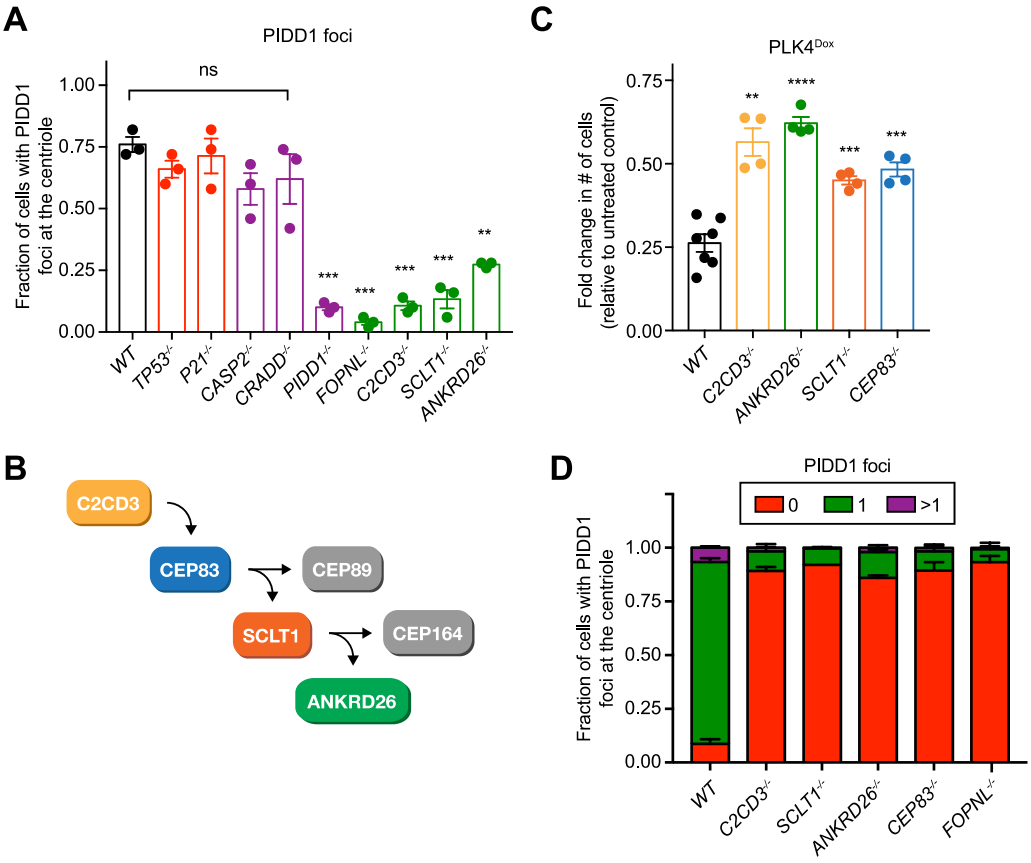
A
PIDD1 foci
ns
Fraction of cells with PIDD1 foci at the centriole
1.00
0.75
0.50
0.25
0.00
WT
TP53-/-
P21-/-
CASP2-/-
CRADD-/-
PIDD1-/-
FOPNL-/-
C2CD3-/-
SCLT1-/-
ANKRD26-/-
C
PLK4Dox
Fold change in # of cells (relative to untreated control)
0.75
0.50
0.25
0.00
WT
C2CD3-/-
ANKRD26-/-
SCLT1-/-
CEP83-/-
B
C2CD3
CEP83
CEP89
SCLT1
CEP164
ANKRD26
D
PIDD1 foci
0
1
>1
Fraction of cells with PIDD1 foci at the centriole
1.00
0.75
0.50
0.25
0.00
WT
C2CD3-/-
SCLT1-/-
ANKRD26-/-
CEP83-/-
FOPNL-/-

Figure 3.2: Distal appendages are required for PIDD1 recruitment and PIDDosome activation. **A.** Quantification of the fraction of cells with PIDD1 localized to the mature mother centriole in PLK4^{Dox} cells expressing an sgRNA targeting the indicated genes. A dot displays measurements from each experiment. Experiments were performed in PLK4^{Dox} polyclonal knockout cells. Data acquired across n = 3 biological replicates. Mean ± s.e.m. **B.** Schematic depicting the hierarchy of recruitment of distal appendage proteins. **C.** Graph showing the relative growth of doxycycline treated PLK4^{Dox} cells that were knocked out for the indicated genes. Each dot displays measurements from a single experiment. Experiments were performed in PLK4^{Dox} monoclonal knockout cells. Data acquired across n ≥ 3 biological replicates. Mean ± s.e.m. **D.** Quantification of the fraction of cells with PIDD1 localized at the mature mother centriole. Experiments were performed in PLK4^{Dox} monoclonal knockout cells. Data acquired across n = 3 biological replicates. Mean ± s.e.m. Data information: Asterisks indicate statistically significant differences between measurements (**: P<0.01; ***: P<0.001, ****: P<0.0001). Statistics for all Figures were calculated using a two-tailed Student's t-test.

Figure 3.3

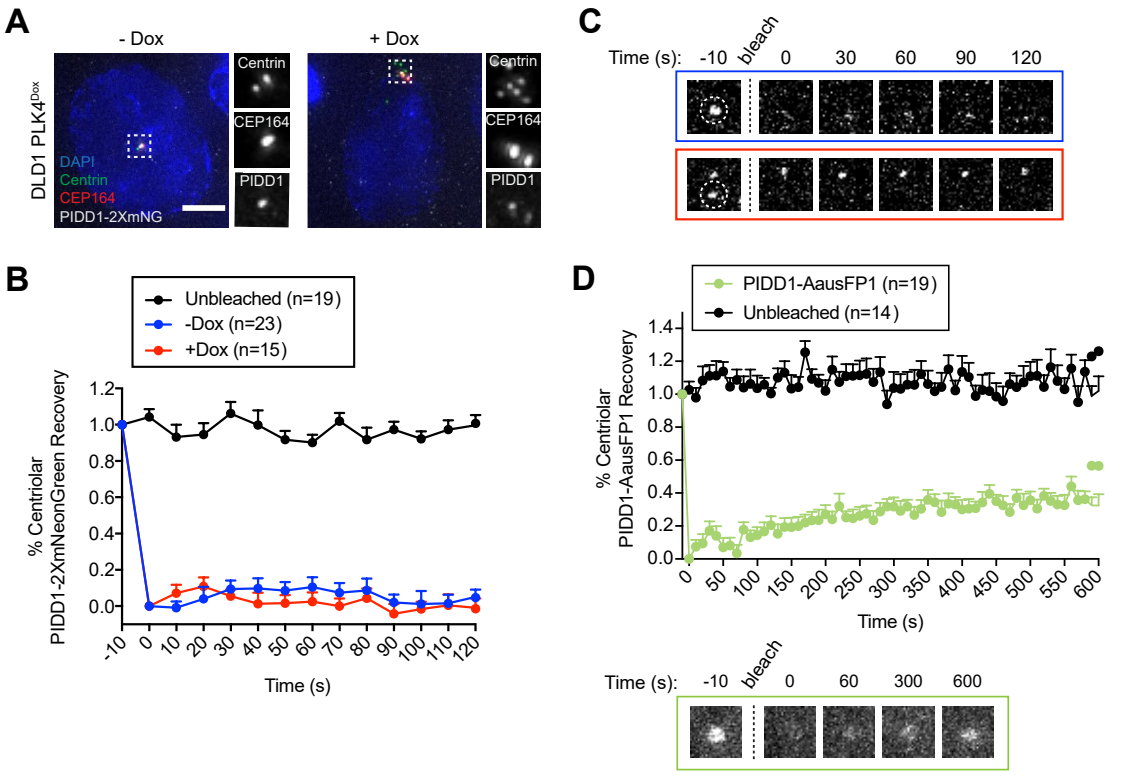

Figure 3.3 PIDD1 stably interacts with centriole distal appendages. **A.** Representative image of PIDD1-2XmNeonGreen in endogenously tagged DLD1 cells. Scale bar = 5 μm. **B.** Quantification of fluorescence recovery after photobleaching. Data acquired across n ≥ 15 cells per condition. Mean + s.e.m. **C.** Representative images of the PIDD1-2XmNeonGreen foci in cells with and without centriole amplification before bleaching, immediately after bleaching and at selected points during the recovery period. **D.** Top: Quantification of fluorescence recovery after photobleaching. Data acquired across n ≥ 14 cells per condition. Mean + s.e.m. Bottom: Representative images of the PIDD1-AausFP1 foci in cells before bleaching, immediately after bleaching and at selected points during the recovery period.

Chapter 4: ANKRD26 is required for PIDDosome activation following centriole amplification

4.1 Introduction

Ankyrin repeat domain 26 (ANKRD26) is a recently identified distal appendage protein that localizes to the periphery of the distal appendages.[49] Prior to its identification at distal appendages and its characterization in the response to supernumerary centrioles[44,45], little was known about the function of ANKRD26. Mutations in ANKRD26 have been identified in patients with thrombocytopenia[53], which is a condition where an abnormally low number of platelets are produced. Most of the mutations in ANKRD26 identified in families with thrombocytopenia occur in the 5' untranslated region (UTR).[54] These mutations in the 5' UTR of ANKRD26 silence its transcriptional repression and lead to constitutive expression in megakaryocytes (platelet producing cells).[53]

Disruption of the Ankrd26 gene in mice has been shown to cause hyperphagia and obesity.[55] This phenotype is cause by a defect in primary cilia formation in the central nervous system, leading to dysregulation of appetite and energy homeostasis.[56] However, whether this phenotype is related to the role of ANKRD26 at the centriole distal appendage or its function in response to extra centrioles is not yet known.

4.2 Methods

4.2.1 Cytokinesis failure assay

To look at the effects of cytokinesis failure, PLK4^{Dox} cells were seeded in duplicate wells. One well was treated with 10 µg/mL cytochalasin B (Sigma-Aldrich) and the other well was treated with DMSO for 24 hrs. Cells were then washed with media 3 times and then fresh media was added to cells supplemented with 10 µM EdU (Invitrogen) and 10 µM Dimethylenastron (DMN) (Sigma-Aldrich). Cells were incubated for 24 hrs. Cells were then collected and fixed with 100% ethanol at -20 ºC for at least 1 hr. Each sample was washed with PBS then stained with a Click-iT reaction for 30 min in the dark. The Click-iT reaction was prepared following manufacturer's protocol (Invitrogen). Samples were washed and stained with a 25 µg/mL propidium iodide solution supplemented with RNase A (Sigma-Aldrich) for 30 min in the dark. Samples were analyzed on a BD FACSCalibur flow cytometer to determine DNA content and EdU incorporation. The percent of EdU-positive cells with a DNA content of greater than 4N was determined for each sample. The DMSO-treated sample was subtracted from the cytochalasin B- treated sample for each cell line.

4.2.2 Griseofulvin assay

PLK4^{Dox} cells were grown on 18-mm glass coverslips and treated with griseofulvin (Sigma-Aldrich, 25 µM) for 24 hr. Cells were then fixed in 100 % -20 °C methanol for 10 min and processed for immunofluorescence staining. Anaphase cells were imaged, and spindle morphology scored.

4.2.3 Cilia assembly

hTERT RPE1 cells were grown to confluency on 18-mm glass coverslips and then placed in serum-free media (DMEM:F12 50:50 medium supplemented with 0.348% sodium bicarbonate, 100 U/ml penicillin, 100 U/ml streptomycin, and 2 mM L-glutamine) for 2 days. Prior to fixation, cells were washed with 1 X PBS and incubated in microtubule stabilization buffer (30% glycerol, 100 mM PIPES, 1 mM EGTA, 1 mM MgSO4) for 30 sec. Cells were then washed with PBS and processed for immunofluorescence staining.

4.2.4 Immunoblotting

Immunoblotting and immunofluorescence were performed as previously described.[57] For immunoblot analysis, protein samples were separated by SDS-PAGE, transferred onto nitrocellulose membranes with a Trans-Blot Turbo Transfer System (BioRad) or by overnight wet-transfer (25 V for 16 hrs in the cold room). For semi-dry transfer, buffer containing 25.3 mM Tris Base, 0.19M glycine and 20 % methanol. For wet-transfer, 25 mM Tris Base, 190 mM glycine, 0.1 % (w/v) SDS and 20 % methanol. Blots were probed with the following antibodies: alpha-tubulin (rat, Y1/2, Invitrogen, MA180017, 1:1000), ANKRD26 (rabbit, GeneTex, GTX128255, 1:1000), Caspase 2 (rat, 11B4, Millipore Sigma, MAB3507, 1:1000), and p21WAF1 (mouse, Ab-1, CalBiochem, OP64, 1:100). Blots were blocked with 5% milk in TBST and washed with TBST. Images were captured on a Syngene G:Box.

4.2.5 Co-immunoprecipitation

Co-immunoprecipitation was performed as previously described.[57] 2 x 10^6 HEK293FT cells were seeded into 10 cm^2 dishes and 24 hours later were transfected with 3 µg of plasmid DNA. 48 hours later, transfected cells were lysed in lysis buffer (10 mM Tris pH 7.5, 0.1% Triton X-100, 250 mM NaCl, 1 mM EDTA, 50 mM NaF, 50 mM β-glycerophosphate, 1 mM DTT, 500 nM microcystin, 1 mM PMSF and EDTA-free protease inhibitor tablet (Roche)), sonicated and soluble extracts prepared. The supernatant was incubated with beads coupled to GFP-binding protein.[58] Beads were washed 3 times in lysis buffer, and immunopurified protein was analyzed by immunoblot.

4.2.6 Immunofluorescence

For immunofluorescence, cells were grown on 18-mm glass coverslips and fixed in 100 % −20 °C methanol for 10 min. Cells were blocked in 2.5 % FBS, 200 mM glycine, and 0.1 % Triton X-100 in PBS for 1 h. Antibody incubations were conducted in the blocking solution for 1 h. DNA was detected using DAPI, and cells were mounted in Prolong Antifade (Invitrogen). Staining was performed with the following primary antibodies: Centrin (rabbit, directly conjugated,[59] 1:1,000), ANKRD26 (rabbit, GeneTex, GTX128255, 1:1000), SCLT1 (rat,[5] 1:250), CEP83 (rabbit, Sigma-Aldrich, HPA038161, 1:200), CEP89 (rat,[5] 1:500), Polyglutamylation (mouse, GT335, AdipoGen, AG-20B-0020-C100), FOPNL/FOR20 (rat,[60] 1:500), C2CD3 (rabbit, Atlas Antibodies, HPA038552, 1:500), and CEP164 (rabbit, Millipore Sigma, AEB2621, 1:1,000). Secondary

donkey antibodies were conjugated to Alexa Fluor® 488, 555, or 650 (Life Technologies).

Immunofluorescence images were collected using a Deltavision Elite system (GE Healthcare) controlling a Scientific CMOS camera (pco.edge 5.5). Acquisition parameters were controlled by SoftWoRx suite (GE Healthcare). Images were collected at room temperature using an Olympus 60× 1.42 NA or Olympus 100× 1.4 NA oil objective at 0.2 μm *z*-sections and subsequently deconvolved in SoftWoRx suite. Images were acquired using Applied Precision immersion oil (*N* = 1.516).

4.2.7 Edu Incorporation

PLK4^{Dox} cells were seeded in duplicate wells and one was treated with one of the following drugs: doxorubicin (Sigma-Aldrich, 50 ng/μL) for 2 days, reversine (Sigma-Aldrich, 500 nM) for 2 days, centrinone (Tocris, 125 nM) for 5 days or H_2O_2 (30% w/w Sigma-Aldrich, 150 nM) for 2 h followed by an overnight incubation in fresh media. Both the treated and untreated wells were seeded onto 18-mm glass coverslips and incubated in media supplemented with 10 μM EdU for 24 h. Cells were then fixed in 100 % −20 °C methanol for 10 min, washed with PBST and a Click-iT reaction was performed for 30 min in the dark to label EdU. Each coverslip was incubated with 197.2 μl 1× PBS, 2.5 μl 100 mM $CuSO_4$, 50 μl 500 mM Ascorbic Acid (prepared fresh), and 0.3 μl 125 μM Azide-fluor 488 (Millipore Sigma). After 30 min, cells were rinsed with PBS, DAPI stained, and then mounted with Prolong Antifade.

4.3 Results

4.3.1 ANKRD26 loss allows for the long-term growth of cells with centriole amplification

In accord with its localization to the peripheral region of the distal appendage blade, ANKRD26 localization at mature centrioles was abolished in *C2CD3*$^{-/-}$, *SCLT1*$^{-/-}$, and *CEP83*$^{-/-}$ cells. Moreover, knocking-out FOPNL also prevented ANKRD26 and PIDD1 recruitment to the centriole, suggesting that while not a distal appendage protein perse, FOPNL plays a role in the assembly of the centriole distal appendages. Conversely, *ANKRD26*$^{-/-}$ cells had a normal distal appendage localization of CEP83, SCLT1, CEP89, and CEP164. Centriole distal appendages are known to play a role in membrane docking of the basal body and ciliogenesis. These functions were not disrupted in *ANKRD26*$^{-/-}$ cells, which formed cilia upon serum starvation at a frequency comparable to wild-type RPE1 cells (Figure 4.1). These data suggest that the distal appendage remains mostly intact in cells lacking ANKRD26.

Knockout of *ANKRD26* allowed for the long-term growth of cells with extra centrioles generated by overexpression of PLK4 (Figure 4.1). To further test if ANKRD26 suppresses the proliferation of cells with extra centrioles, we used two additional methods to drive the formation of excessive centrioles that did not require overexpression of PLK4. First, overexpression of the centriole structural component SAS6 led to centrosome amplification that reduced cell proliferation.[31] This decrease in proliferation was alleviated by knockout of ANKRD26. Second, we treated cells with cytochalasin B to induce cytokinesis failure and tested the

ability of ANKRD26, PIDD1 and CASP2 to arrest the proliferation of tetraploid cells that have twice the normal centrosome content. Knockout of ANKRD26, PIDD1 or CASP2 increased the fraction of cycling tetraploid cells, indicating that all three of these genes act to restrict the proliferation of newly created tetraploid cells. We note that the relative increase in growth following loss of ANKRD26 in tetraploid cells was more modest than what was observed in cells with extra centrosomes generated by PLK4 overexpression. This may reflect the shorter duration of the growth assays performed in tetraploid cells (2 days) compared to those carried out in PLK4^{Dox} cells (5 days). Alternatively, tetraploid cells may activate other ANKRD26-independent pathways that restrict cell proliferation.[32]

Importantly, ANKRD26 was not required for normal centriole duplication, as *ANKRD26*$^{-/-}$ cells experienced robust centriole amplification when PLK4 was overexpressed. To test if the extra centrosomes in *ANKRD26*$^{-/-}$ cells could act as microtubule organizing centers (MTOCs), we treated PLK4^{Dox} cells with dox for two days and then added the centrosome de-clustering agent griseofulvin.[61] As expected, extra centrosomes in both wild-type and *ANKRD26*$^{-/-}$ cells nucleated microtubules that led to multi-polar divisions in the presence of griseofulvin. We conclude that ANKRD26 is required to restrict the proliferation of cells following centrosome amplification but is not required for cilia assembly, centriole duplication, or PCM recruitment.

4.3.2 ANKRD26 links extra centrosomes to PIDDosome activation

To test the effect of ANKRD26 knockout on PIDDosome activation, we monitored the loss of pro-CASP2 and the upregulation of P21 upon centrosome

amplification. As expected[30], the levels of pro-CASP2 decreased, and P21 increased in PLK4^{Dox} cells in a time-dependent manner following dox addition (Figure 4.2). Knockout of TP53 prevented P21 upregulation but did not affect pro-CASP2 processing following centrosome amplification, which is consistent with its position downstream of CASP2 in the pathway. By contrast, knockout of ANKRD26 suppressed both CASP2 activation and P21 upregulation in cells with extra centrosomes. These data show ANKRD26 acts as an upstream activator of the PIDDosome and CASP2 in cells with supernumerary centrosomes.

CASP2 is activated in response to several different upstream signals.[62] To investigate if the loss of ANKRD26 globally prevents CASP2 activation, we tested the ability of *ANKRD26*$^{-/-}$ and *TP53*$^{-/-}$ cells to activate CASP2 following DNA damage induced by etoposide. While the loss P53 prevented P21 expression downstream of CASP2 activation, knockout of ANKRD26 did not alter CASP2 activation or P21 induction in cells that experienced DNA damage (Figure 4.2). This suggests that ANKRD26 is required to activate CASP2 in cells with extra centrosomes but is not required for CASP2 function perse. Notably, CASP2 processing still occurred in *PIDD1*$^{-/-}$ cells treated with etoposide, suggesting that etoposide-induced CASP2 activation is independent of the PIDDosome.

We next investigated if ANKRD26$^{-/-}$ cells were defective in other P53-dependent response pathways. Knockout of *ANKRD26*$^{-/-}$ did not affect the ability of cells to arrest following DNA damage, centrosome loss, and chromosome segregation errors. Moreover, *ANKRD26*$^{-/-}$ cells underwent H_2O_2-induced arrest at similar levels to control cells. By contrast, *TP53*$^{-/-}$ cells exhibited enhanced

growth in all of these conditions. Since upstream components of the DNA damage and senescence pathways did not emerge as hits in our screen, we conclude that ANKRD26-mediated activation of P53 only occurs following centriole amplification and is functionally distinct from the DNA damage and senescence response pathways.

4.3.3 The ANKRD26 coiled-coil region interacts with the UPA domain of PIDD1

To determine which region of ANKRD26 is required to recruit PIDD1 to centriole distal appendages, we expressed deletion mutants of mCherry-ANKRD26 in *ANKRD26*$^{-/-}$ cells and monitored PIDD1 recruitment to the centriole. The deletion of the ANKRD26 N- terminus (amino acids 1-344) led to a partial reduction in the centriole recruitment of ANKRD26 and PIDD1. In contrast, deletion of the ANKRD26 C- terminus (amino acids 1231-1710) prevented the centriole localization of both proteins (Figure 4.3). This suggests that the N and C-terminal region of ANKRD26 both play a role in its own centriole recruitment.

The deletion of the ANKRD26 M1 region (amino acids 345-849) had no impact on the centriole recruitment of ANKRD26, but partly compromised the centriole localization of PIDD1. Notably, deletion of ANKRD26 M2 (amino acids 850-1320) localized to the centriole, but completely failed in the recruitment of PIDD1 (Figure 4.3). These data indicate that the 850-1320 amino acid region of ANKRD26 is required for the recruitment of PIDD1 to the centriole distal appendage.

The 850-1320 amino acid region of ANKRD26 contains a conserved coiled-coil region (CCDC144C, amino acids 913-1216). To establish if this coiled-coil region is responsible for binding to PIDD1, we overexpressed in cells with a normal centrosome content mCherry-ANKRD26 coiled-coil (mCherry-ANKRD26^{CC}) and wild-type PIDD1- FLAG. Purified mCherry-ANKRD26^{CC} associated with PIDD1-FLAG, showing that the coiled-coil region of ANKRD26 is sufficient for PIDD1 binding.

Full-length PIDD1 is processed into three fragments: an N-terminal piece called PIDD1-N and two C-terminal fragments, PIDD1-C and PIDD1-CC, respectively.[36,63] Cleavage occurs at S446 and S588 through an autoproteolytic process similar to the mechanism described by self-cleaving protein segments such as inteins. Full-length PIDD1 is rapidly processed in cells to form PIDD1-C, while the second cleavage event that forms the PIDD1-CC fragment is stimulated by specific inputs.[63] To define the region of PIDD1 that interacts with ANKRD26, we expressed in cells mCherry- ANKRD26^{CC} along with FLAG-tagged PIDD1-N, PIDD1-C, and PIDD1-CC. mCherry- ANKRD26^{CC} interacted with the PIDD1-C and PIDD1-CC fragments but failed to bind PIDD1-N (Figure 4.3). Importantly, ANKRD26^{CC} did not bind to PIDD1 lacking the CC fragment (PIDD1 ΔCC), demonstrating that the CC fragment of PIDD1 is both necessary and sufficient for ANKRD26 binding.

The PIDD1-CC region contains a UPA domain of unknown function[64] and a death domain (DD) that binds to CRADD to form the PIDDosome.[52] To establish which of these domains are responsible for associating with ANKRD26,

we tested the ability of PIDD1 mutants lacking the UPA domain or DD to bind to ANKRD26^{CC}. ANKRD26^{CC} robustly interacted with PIDD1 lacking the DD (PIDD1ΔDD), but only weakly associated with PIDD1 deleted of the UPA domain (PIDD1ΔUPA). This suggests that the coiled-coil region of ANKRD26 predominantly associates with the PIDD1 UPA domain.

Additionally, a non-cleavable mutant of PIDD1 retained its ability to interact with ANKRD26^{CC}, arguing that PIDD1 cleavage is not required to bind to ANKRD26. In fact, ANKRD26^{CC} preferentially binds to unprocessed, full-length PIDD1.

4.3.4 ANKRD26-mediated recruitment of PIDD1 to the distal appendage is required for PIDDosome activation

To test the role of ANKRD26-mediated recruitment of PIDD1 in activating the PIDDosome, we expressed a mCherry-ANKRD26 or mCherry-ANKRD26ΔCC transgene in *ANKRD26*$^{-/-}$ PLK4^{Dox} cells. Expression of a wild-type mCherry-ANKRD26 transgene was able to rescue PIDD1 recruitment to the mature parent centrioles. Furthermore, wild-type mCherry-ANKRD26 promoted PIDDosome activation and suppressed the proliferation of cells with extra centrioles. By contrast, although the mCherry-ANKRD26ΔCC mutant localized to the centriole, it could not recruit PIDD1 to the distal appendage. Importantly, the mCherry-ANKRD26ΔCC mutant did not restrict proliferation in cells with extra centrioles, nor did it induce PIDDosome activation. This suggests that ANKRD26-mediated recruitment of PIDD1 to the distal appendage is required for PIDDosome activation and growth arrest following centriole amplification.

4.3.5 A recurrent cancer mutation disrupts the ability of ANKRD26 to arrest the proliferation of cells with extra centrioles

We investigated whether defects in ANKRD26-mediated PIDDosome activation occur in human cancers. Interestingly, a single nucleotide deletion in ANKRD26 was found in 20 independent tumors from the colon, stomach, uterus, and brain (Figure 4.4).[42] This one base pair deletion resulted in a K1234N mutation and a premature translational stop that truncated ANKRD26 just after the CC domain that interacts with PIDD1. The striking recurrence of the same mutation suggests that the K1234Nfs*19 alteration is selected for in these cancers. To test the impact of this mutation on ANKRD26-mediated PIDDosome activation, we expressed a mCherry- ANKRD26 K1234Nfs*19 transgene in *ANKRD26*$^{-/-}$ PLK4^{Dox} cells.

Similar to what was observed following the deletion of the ANKRD26 C-terminus (amino acids 1231-1710), the mCherry-ANKRD26 K1234Nfs*19 mutant localized inefficiently to the centriole and was defective in recruiting PIDD1 to the distal appendage (Figure 4.4). This mutant also failed to promote PIDDosome activation and restrict the proliferation of cells with extra centrosomes. This suggests that the K1234Nfs*19 mutation disrupts the ability of ANKRD26 to localize to the centriole and trigger PIDD1 activation following centrosome amplification.

P53 functions downstream of ANKRD26 to arrest the growth of cells with extra centrosomes. Given that P53 loss of function frequently occurs in human tumors and would be expected to overcome the requirement for ANKRD26-

disrupting mutations, we analyzed the fraction of ANKRD26 K1234Nfs*19 tumors that also showed oncogenic *TP53* alterations. Of the 20 tumors containing K1234N mutations, 15 % also contained an oncogenic *TP53* alteration, and an additional 15 % have a *TP53* variant of unknown significance (Table 4.1). This fraction is lower than the overall frequency of *TP53* alterations observed for each tumor type subtype. However, since the numbers of tumors analyzed are small, no definitive conclusions can be drawn at this stage.

4.4 Discussion

ANKRD26 is required for PIDD1 recruitment to the centriole and PIDDosome activation following centriole amplification induced either by PLK4 overexpression or cytokinesis failure. Loss of ANKRD26 prevented downstream stabilization of P53 in cells with extra centrioles, but other cellular stress responses remained intact. These data indicate that ANKRD26 is uniquely involved in initiating a P53-dependent arrest in response to centriole amplification.

Loss of ANKRD26 allows for the continued proliferation of genetically unstable cells with centriole amplification. This raises the question of whether mutations in *ANKRD26* are selected for during the process of tumorigenesis. We predict that loss of ANKRD26 would offer no fitness advantage in tumor cells that lack P53 functionality, perhaps explaining why *ANKRD26* mutations are not commonly observed in human cancers. Nevertheless, a query of the cBioPortal database did reveal a recurrent frameshift mutation in *ANKRD26* (K1234Nfs*19)

observed in multiple stomach, brain, uterine, and colon tumors.[42] This mutation leads to the expression of a truncated form of ANKRD26 that fails to recruit PIDD1 to the centriole and activate the PIDDosome in response to centriole amplification. This suggests that loss of ANKRD26-mediated PIDD1 signaling is selected for in some human tumors. It is plausible that the K1234Nfs*19 *ANKRD26* mutation enables the continued propagation of tumor cells with extra centrioles. It would be interesting to examine if selection for this mutation co-occurs with centriole amplification in cancer cells.

In addition to a possible role of *ANKRD26* mutations in tumorigenesis, mutations in the 5' UTR of the *ANKRD26* gene cause an autosomal-dominant form of thrombocytopenia due to reduced blood platelet production by megakaryocytes.[65,66] During their maturation, megakaryocytes undergo several rounds of endomitosis (mitosis without cytokinesis) to produce large polyploid cells with extra centrosomes.[67] Thrombocytopenia-associated mutations in *ANKRD26* lead to the persistent expression of *ANKRD26* during the late stages of megakaryocyte development, and, consequently, megakaryocytes from these patients exhibit reductions in cell ploidy.[53] Based on our observations regarding the role of ANKRD26 in responding to centriole amplification, it is tempting to speculate that the reduction in megakaryocyte ploidy in these patients arises due to ANKRD26-mediated activation of the PIDDosome in megakaryocytes with extra centrioles. Patients with mutations in the 5′ UTR of *ANKRD26* also exhibit an increased incidence of myeloid malignancies[65,66,68], and N-terminal truncating mutations in ANKRD26 have been identified in

sporadic, adult-onset AML cases.[54] How these ANKRD26 mutations lead to an increased incidence of hematological malignancies, however, remains unclear.

4.5 Tables for Chapter 4

Table 4.1: *TP53* mutational status of tumors containing the ANKRD26 K1234Nfs*19 mutation

Sample ID	Type of cancer	TP53 mutation	TP53 copy number	Likely oncogenic	TP53 alteration frequency in tumor subtype
pfg143T	Stomach Adenocarcinoma	None	Not available	N/A	49%
coadread_dfci_2016_1748	Colorectal Adenocarcinoma	None	Not available	N/A	65%
coadread_dfci_2016_189255	Colorectal Adenocarcinoma	None	Not available	N/A	65%
coadread_dfci_2016_261	Colorectal Adenocarcinoma	None	Not available	N/A	65%
coadread_dfci_2016_341	Colorectal Adenocarcinoma	None	Not available	N/A	65%
coadread_dfci_2016_224049	Colorectal Adenocarcinoma	None	Not available	N/A	65%
TCGA-CM-4743	Colon Adenocarcinoma	None	None	N/A	56%
TCGA-B7-5816	Diffuse Type Stomach Adenocarcinoma	None	None	N/A	49%
TCGA-CG-4305	Stomach Adenocarcinoma	None	None	N/A	49%
TCGA-AJ-A2QO	Uterine Endometrioid Carcinoma	None	None	N/A	38%
TCGA-AX-A1C4	Uterine Endometrioid Carcinoma	None	None	N/A	38%
TCGA-B5-A0JZ	Uterine Endometrioid Carcinoma	None	None	N/A	38%
TCGA-BR-4368	Stomach Adenocarcinoma	None	None	N/A	49%
GIS003-HK-pfg143	Stomach Adenocarcinoma	None	Not available	N/A	49%
01CO022	Colon Adenocarcinoma	None	Amplification	Unknown	65%
TCGA-HU-A4GX	Diffuse Type Stomach Adenocarcinoma	P72S	None	Unknown	49%
TCGA-VQ-A8PP	Tubular Stomach Adenocarcinoma	V97D	None	Unknown	49%

TCGA-DI-A1BU	Uterine Mixed Endometrial Carcinoma	K382Nfs*40	None	Yes	38%
coadread_dfci_2016_207430	Colorectal Adenocarcinoma	P36Afs*7	Not available	Yes	65%
TCGA-HT-8564	Astrocytoma	R267Q/R156H	Shallow Deletion	Yes	38%

4.6 Figures for Chapter 4

Figure 4.1

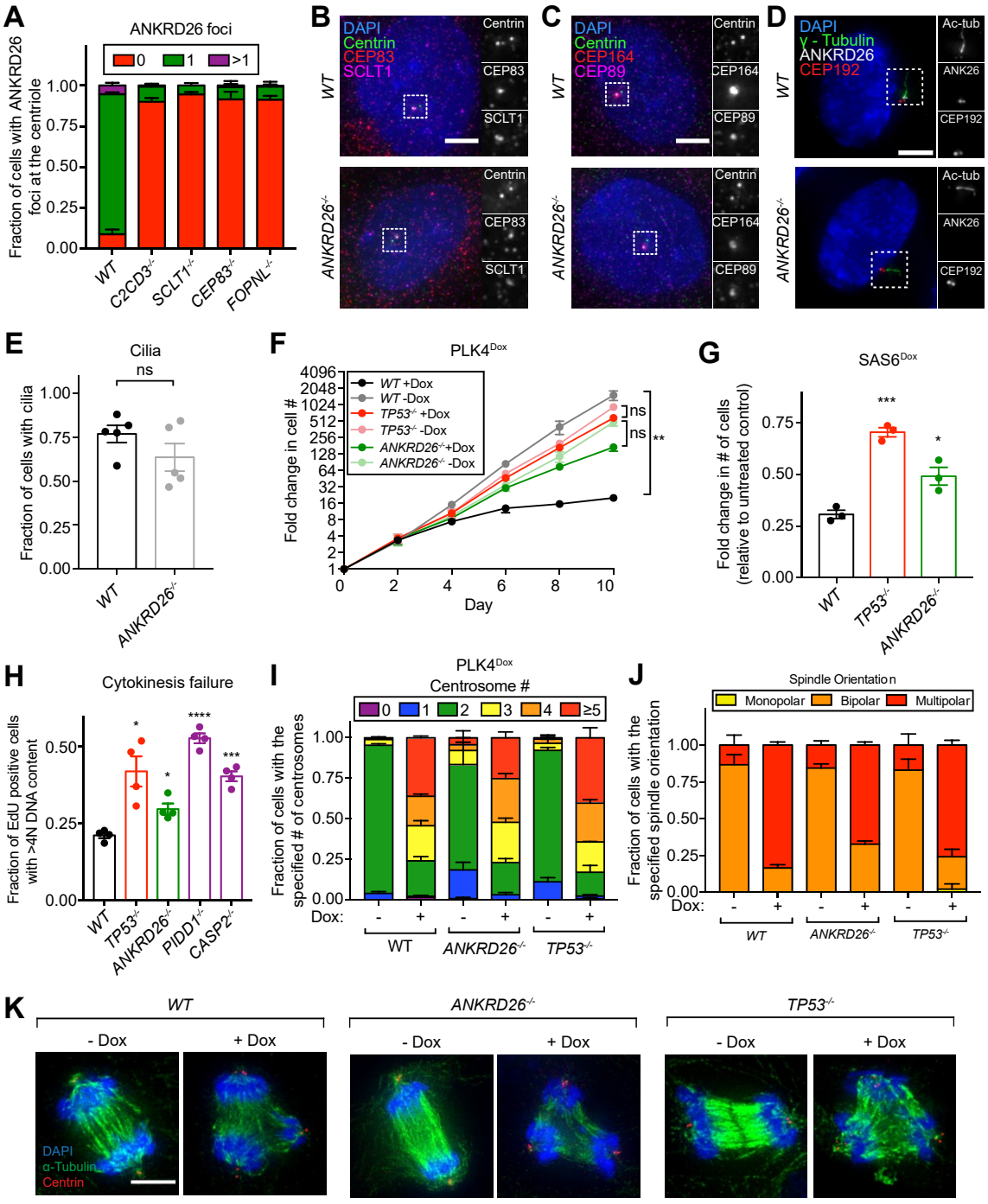

Figure 4.1 ANKRD26 is uniquely involved in the response to centriole amplification. **A.** Quantification of the fraction of cells with ANKRD26 localized at the mature mother centriole. Experiments were performed in PLK4^{Dox} monoclonal knockout cells. Data acquired across *n* = 3 biological replicates. Mean ± s.e.m. **B-D.** Representative images of *WT* or *ANKRD26*$^{-/-}$ cells immunostained with the indicated antibodies. Scale bar = 5 μm. **E.** Quantification of the fraction of *WT* or *ANKRD26*$^{-/-}$ hTERT RPE1 cells with cilia. Each dot displays measurements from a single experiment. Data acquired across *n* = 5 biological replicates. Mean ± s.e.m. **F.** Growth assay of the indicated cells with and without doxycycline-inducible overexpression of PLK4. Experiments were performed in PLK4^{Dox} monoclonal knockout cells. Data acquired across *n* = 3 biological replicates. Mean ± s.e.m. **G.** Graph showing the relative growth of doxycycline-treated SAS6^{Dox} cells that were knocked out for the indicated genes. Experiments were performed in SAS6^{Dox} monoclonal knockout cells. Each dot displays measurements from a single experiment. Data acquired across *n* = 3 biological replicates. Mean ± s.e.m. **H.** Quantification of the fold change in cycling cells with a DNA content > 4N following cytokinesis failure. Experiments were performed in PLK4^{Dox} monoclonal knockout cells. Each dot displays measurements from a single experiment. Data acquired across *n* = 4 biological replicates. Mean ± s.e.m. **I.** Quantification of centrosome number in PLK4^{Dox} cells expressing an sgRNA targeting the indicated genes. Experiments were performed in PLK4^{Dox} monoclonal knockout cells. Data acquired across *n* = 3 biological replicates. Mean ± s.e.m. **J.** Quantification of the fraction of cells with

the indicated mitotic spindle orientation following treatment with the centrosome declustering agent griseofulvin. Experiments were performed in monoclonal PLK4^{Dox} knockout cells. Data acquired across *n* = 3 biological replicates. Mean ± s.e.m. K. Representative images of PLK4^{Dox} cells treated with and without doxycycline for two days then treated with griseofulvin for 24 h. Experiments were performed in monoclonal PLK4^{Dox} knockout cells. Cells were immunostained with indicated antibodies. Scale bar = 5 μm.

Figure 4.2

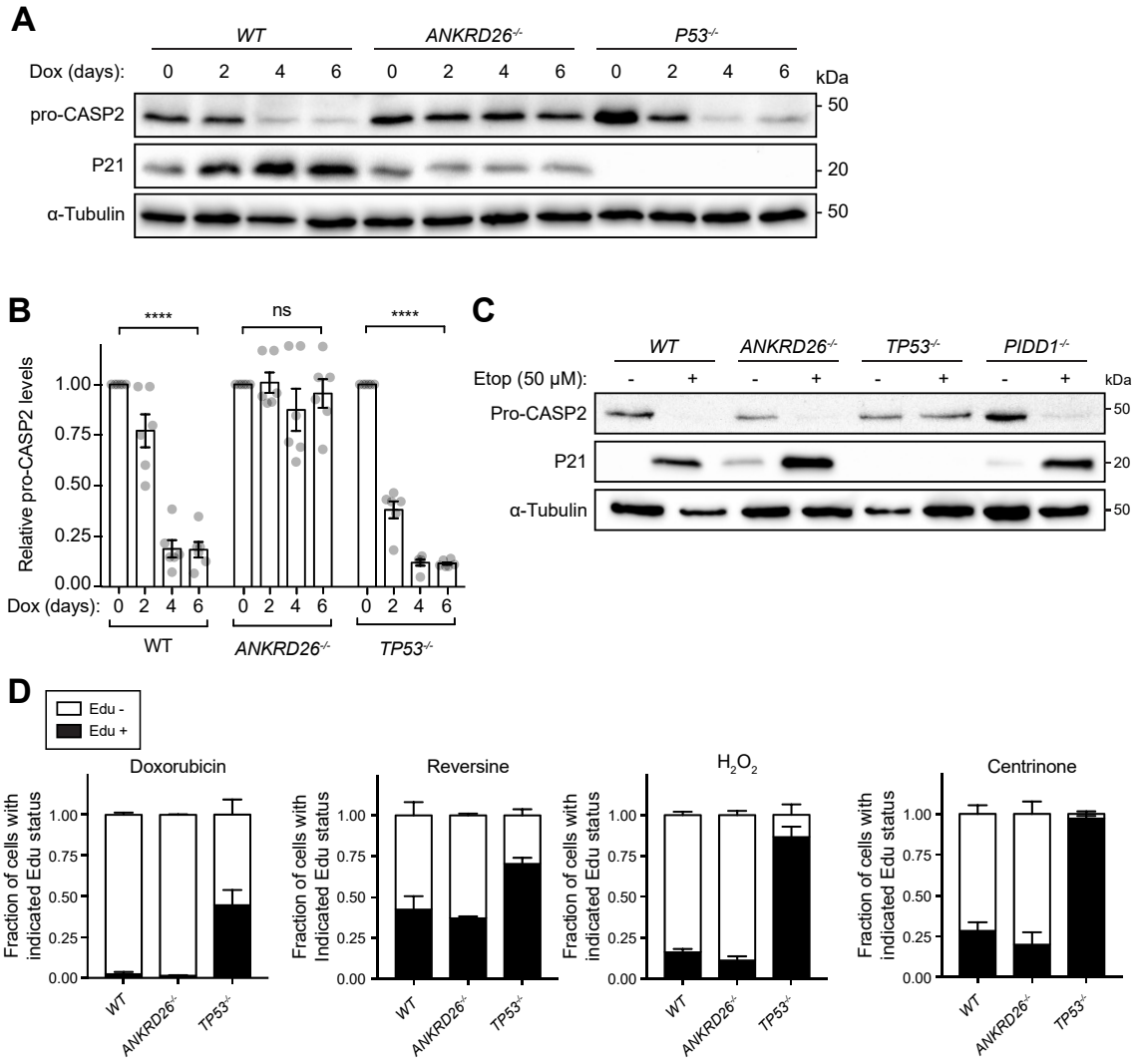
A
WT
ANKRD26-/-
P53-/-
Dox (days): 0 2 4 6 0 2 4 6 0 2 4 6
kDa
pro-CASP2
P21
α-Tubulin
50
20
50
B
****
ns
****
Relative pro-CASP2 levels
1.00
0.75
0.50
0.25
0.00
Dox (days): 0 2 4 6 0 2 4 6 0 2 4 6
WT
ANKRD26-/-
TP53-/-
C
WT
ANKRD26-/-
TP53-/-
PIDD1-/-
Etop (50 μM): - + - + - + - +
kDa
Pro-CASP2
P21
α-Tubulin
50
20
50
D
Edu -
Edu +
Doxorubicin
Reversine
H2O2
Centrinone
Fraction of cells with indicated Edu status
1.00
0.75
0.50
0.25
0.00
WT
ANKRD26-/-
TP53-/-

Figure 4.2 ANKRD26 is required for PIDDosome activation in cells with extra centrioles. **A.** Western blot showing expression of pro-CASP2 and P21 following treatment with dox for the specified number of days. Experiments were performed in PLK4^{Dox} monoclonal knockout cells. **B.** Quantification of pro-CASP2 levels following treatment with dox for the specified number of days. Experiments were performed in PLK4^{Dox} monoclonal knockout cells. Each dot displays measurements from a single experiment. Data acquired across *n* = 6 biological replicates. Mean ± s.e.m. **C.** Western blot showing expression of pro-CASP2 and P21 following treatment with etoposide. Experiments were performed in PLK4^{Dox} cells knocked out for the indicated genes. **D.** Quantification of the fraction of proliferating cells following treatment with the indicated drugs/reagents. Experiments were performed in monoclonal PLK4^{Dox} knockout cells. Data acquired across *n* = 3 biological replicates. Mean ± s.e.m.

Figure 4.3

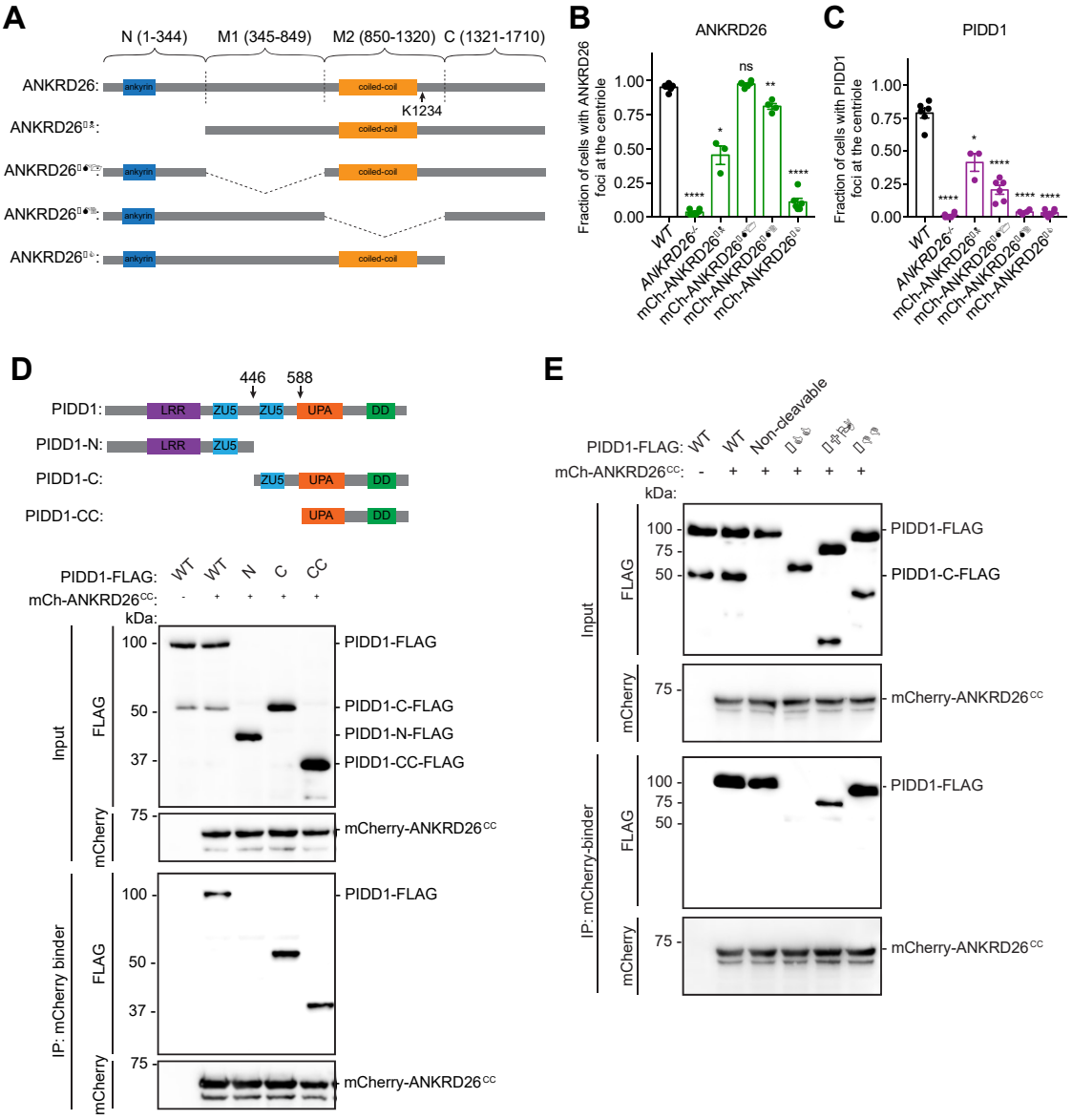
A
N (1-344)
M1 (345-849)
M2 (850-1320)
C (1321-1710)
ANKRD26:
ANKRD26Δ1:
ANKRD26Δ2:
ANKRD26Δ3:
ANKRD26Δ4:
ankyrin
coiled-coil
K1234
B
ANKRD26
Fraction of cells with ANKRD26 foci at the centriole
ns
C
PIDD1
Fraction of cells with PIDD1 foci at the centriole
WT
ANKRD26-/-
mCh-ANKRD26Δ1
mCh-ANKRD26Δ2
mCh-ANKRD26Δ3
mCh-ANKRD26Δ4
D
446
588
PIDD1:
PIDD1-N:
PIDD1-C:
PIDD1-CC:
LRR
ZU5
UPA
DD
PIDD1-FLAG:
mCh-ANKRD26CC:
kDa:
Input
FLAG
mCherry
IP: mCherry binder
PIDD1-FLAG
PIDD1-C-FLAG
PIDD1-N-FLAG
PIDD1-CC-FLAG
mCherry-ANKRD26CC
E
Non-deavable
Input
IP: mCherry-binder

Figure 4.3 The coiled-coil domain of ANKRD26 interacts with the UPA domain of PIDD1 to recruit it to the centriole. **A.** Schematic representation of wild-type ANKRD26 and various mutants. **B.** Quantification of the fraction of cells with ANKRD26 localized to the mature mother centriole in monoclonal *ANKRD26*$^{-/-}$ PLK4^{Dox} cells expressing the indicated mCherry-ANKRD26 transgene. Each dot displays measurements from a single experiment. Data acquired across $n \geq 3$ biological replicates. Mean ± s.e.m. **C.** Quantification of the fraction of cells with PIDD1 localized to the mature mother centriole in monoclonal *ANKRD26*$^{-/-}$ PLK4^{Dox} cells expressing the indicated mCherry-ANKRD26 transgene. Each dot displays measurements from a single experiment. Data acquired across $n = 3$ biological replicates. Mean ± s.e.m. **D.** Top: schematic representation of PIDD1 and its cleavage products. Bottom: HEK293FT cells were transfected with the indicated constructs, subjected to co-immunoprecipitation with mCherry binder beads and immunoblotted with the indicated antibodies. **E.** HEK293FT cells were transfected with the indicated constructs, subjected to co-immunoprecipitation with mCherry binder beads and immunoblotted with the indicated antibodies.

Figure 4.4

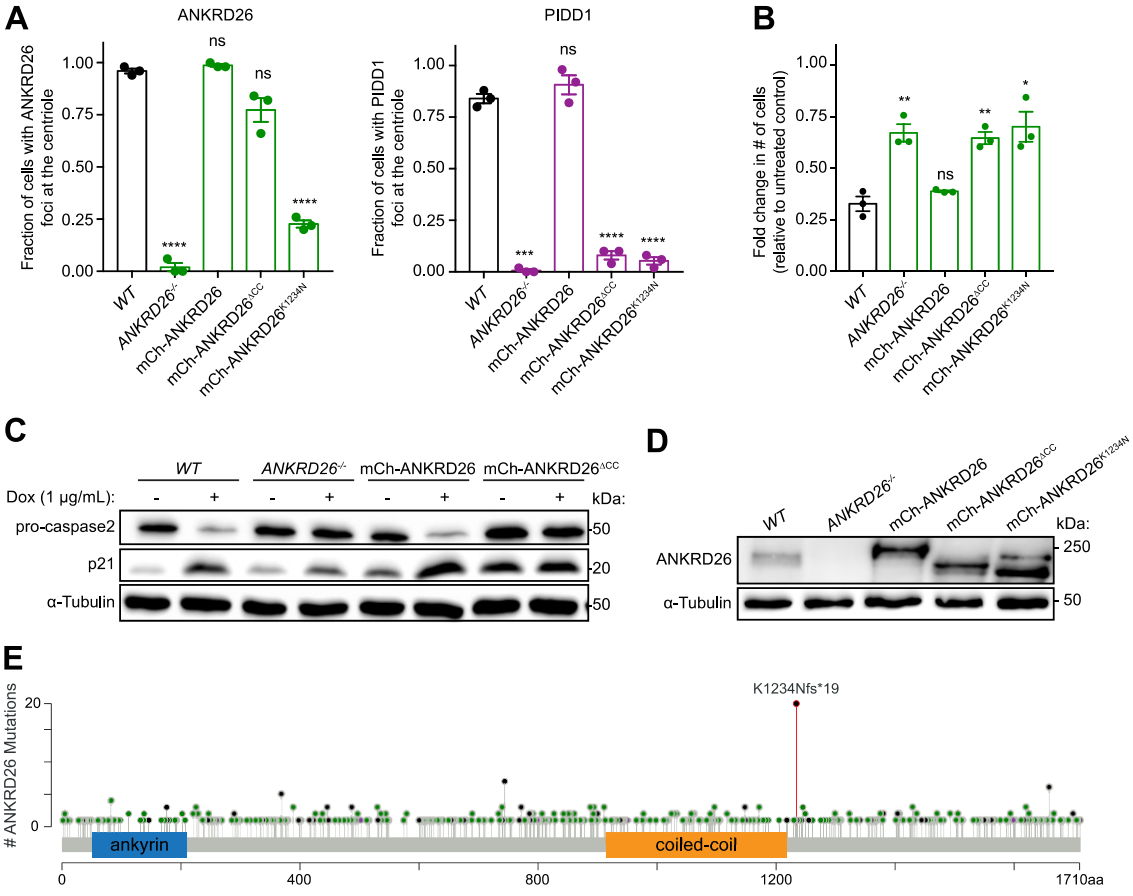
A
ANKRD26
PIDD1
Fraction of cells with ANKRD26 foci at the centriole
Fraction of cells with PIDD1 foci at the centriole
1.00
0.75
0.50
0.25
0.00
ns
****
***
WT
ANKRD26-/-
mCh-ANKRD26
mCh-ANKRD26ΔCC
mCh-ANKRD26K1234N
B
Fold change in # of cells (relative to untreated control)
**
*
C
WT
ANKRD26-/-
mCh-ANKRD26
mCh-ANKRD26ΔCC
Dox (1 μg/mL):
kDa:
pro-caspase2
p21
α-Tubulin
50
20
D
ANKRD26
250
E
ANKRD26 Mutations
20
0
K1234Nfs*19
ankyrin
coiled-coil
0
400
800
1200
1710aa

Figure 4.4 Full-length ANKRD26 is able to rescue PIDD1 recruitment and PIDDosome activation in *ANKRD26*$^{-/-}$ cells. **A.** Quantification of the fraction of cells with ANKRD26 (left) and PIDD1 (right) localized to the mature mother centriole in monoclonal *ANKRD26*$^{-/-}$ PLK4^{Dox} cells expressing the indicated transgenes. Each dot displays measurements from a single experiment. Data acquired across *n* = 3 biological replicates. Mean ± s.e.m. **B.** Graph showing the relative growth of doxycycline-treated, monoclonal *ANKRD26*$^{-/-}$ PLK4^{Dox} cells expressing the indicated ANKRD26 transgenes. Each dot displays measurements from a single experiment. Data acquired across *n* = 3 biological replicates. Mean ± s.e.m. **C.** Western blot showing expression of pro-CASP2 and P21 following treatment with dox for 4 days. Experiments were performed in monoclonal *ANKRD26*$^{-/-}$ PLK4^{Dox} cells expressing the indicated transgenes. **D.** Western blot showing the expression of ANKRD26. Experiments were performed in monoclonal *ANKRD26*$^{-/-}$ PLK4^{Dox} cells expressing the indicated ANKRD26 transgenes. **E.** Schematic showing the location of the 533 mutations in *ANKRD26* in human tumors. Black represents truncating mutations; green represents missense mutations; purple represents inframe mutations. The K1234Nfs*19 mutation is shown in red. Data from curated set of non-redundant studies in cBioPortal.[42]

Chapter 5: Designing a knock-out mouse to study the effects of Ankrd26 loss in vivo

5.1 Introduction

Partial inactivation of Ankrd26 in mice has been achieved by insertion of a β-galactosidase gene into the *Ankrd26* locus using the gene trap technique.[55] This insertion disrupts the C-terminal region of Ankrd26 and leads to a truncation of the *Ankrd26* gene. Animals homozygous for this gene trap allele (*Ankrd26*$^{GT/GT}$) experience hyperphagia, obesity and insulin resistance. This phenotype was found to be caused by region specific changes in primary cilia in the brain, leading to an increased food intake and ultimately obesity.[65]

The mouse *Ankrd26* gene is located on chromosome 6 and consists of 35 exons spanning ~61 Kb. In the Ankrd26 gene trap mice, the β-galactosidase gene was inserted following exon 24, therefore, only the C-terminus of the gene is disrupted. Furthermore, characterization of the *Ankrd26*$^{GT/GT}$ animals showed that they express both mRNA and a protein corresponding to the Ankrd26-β-galactosidase fusion product.[55] Whether this protein retains functional activity or if the *Ankrd26*$^{GT/GT}$ mouse represents a full inactivation of Ankrd26 remains unclear. In order to faithfully study the effects if *Ankrd26* loss *in vivo*, we decided to generate an *Ankrd26*$^{-/-}$ mouse by making a large deletion in the gene using CRISPR.

5.2 Methods

5.2.1 Generation of the *Ankrd26*$^{-/-}$ mouse

CRISPOR[69] was used to optimize sgRNA selection on either side of a 15 Kb region of Ankrd26 (deletion of exons 21-28). A repair template was generated with a BamHI cut site (GGATCC) flanked by 41 bp homology arms. Pronuclear injection was performed by the Transgenic mouse core laboratory at JHU/SOM.

The presence of a deletion in the Ankrd26 gene was assessed by PCR. F Primer: KO_F2 (AAAGTGCCTCCTTCTGCTTG) , R Primer: KO_R4 (CCCCAAAATCTCAGGAATGA). The presence of the WT allele was assessed using F Primer: KO_F3 (TTCCGAGAGCATTTTGTGTG) and R Primer: KO_R3 (CACCCACACACACACTGGAT). The thermocycling parameters for the PCR were: 94 °C for 30 sec, 35 cycles of (94 °C for 30 sec, 55 °C for 30 sec, 72 °C for 60 sec), and 72 °C for 5 min.. PCR product was digested with BamHI at 37 ºC for 2 hrs and run on a 1 % agarose gel. Mice that had insertion of the repair template (evident by BamHI cleavage) were further validated by Sanger sequencing.

5.3 Results

5.3.1 *Ankrd26*$^{-/-}$ mice experience obesity

To see if the *Ankrd26*$^{-/-}$ mice experience an obesity phenotype like the *Ankrd26*$^{GT/GT}$ animals, *Ankrd26* wild-type, heterozygous and homozygous knockout littermates were weighed each week for 40 weeks. *Ankrd26*$^{-/-}$ mice show an increased body weight compared to WT and heterozygous littermates

(Figure 5.1). This deviation was evident earlier in males compared to female animals; beginning at ~7 weeks in males compares to ~10 weeks in females. The differences in weight between *Ankrd26*$^{-/-}$ mice and their littermates was more pronounced in females, however.

5.4 Discussion

The *Ankrd26*$^{-/-}$ mice have a similar obesity phenotype as that reported for *Ankrd26*$^{GT/GT}$ animals.[55] The weight of *Ankrd26*$^{-/-}$ mice was not as high as that observed for *Ankrd26*$^{GT/GT}$ mice, nor was the difference between littermates as striking. However, these discrepancies may be due to the differences in feed used during each experiment. Whether the obesity phenotype observed in the *Ankrd26*$^{-/-}$ animals is due to cilia defects, as has been reported for *Ankrd26*$^{GT/GT}$ mice, has yet to be determined. The consistencies between the two models, lead us to speculate that this is likely the case. Additionally, these results suggests that despite the production of a fusion product, the *Ankrd26*$^{GT/GT}$ mice represent a full knockout of *Ankrd26*.

It would be interesting to see that affect centriole amplification has on *Ankrd26*$^{-/-}$ mice. Previous studies show that centriole amplification alone is sufficient to promote spontaneous tumorigenesis in mice.[24] We would predict that loss of *Ankrd26* and consequent inactivation of the pathway that prevents the proliferation of cells with extra centrioles would accelerate the process of tumorigenesis in animals with centriole amplification.

Loss of PIDDosome components has been shown to lead to an increase in liver ploidy *in vivo*.[70] Liver hepatocytes are natural polyploid and undergo cytokinesis failure during postnatal development.[71] The PIDDosome restricts the ploidy of these cells to mostly 8N, however, when PIDD1, CRADD, CASP2 or P53 are lost, hepatocyte ploidy reaches 16N and even 32N in mice. Our lab has preliminary evidence that loss of *Ankrd26* in both the *Ankrd26*$^{-/-}$ and *Ankrd26*$^{GT/GT}$ mice results in a similar increase in liver ploidy (unpublished). This provides physiological evidence that ANKRD26 functions to restrict the growth of cells with extra centrioles *in vivo*.

Defects in platelet formation or blood clotting has not been observed in either the *Ankrd26*$^{-/-}$ or *Ankrd26*$^{GT/GT}$ animal models. This underscores the idea that the thrombocytopenia-associated mutations in ANKRD26 are likely activating mutations[53] and not the results of a null or hypomorphic gene.

5.5 Figures for Chapter 5

Figure 5.1

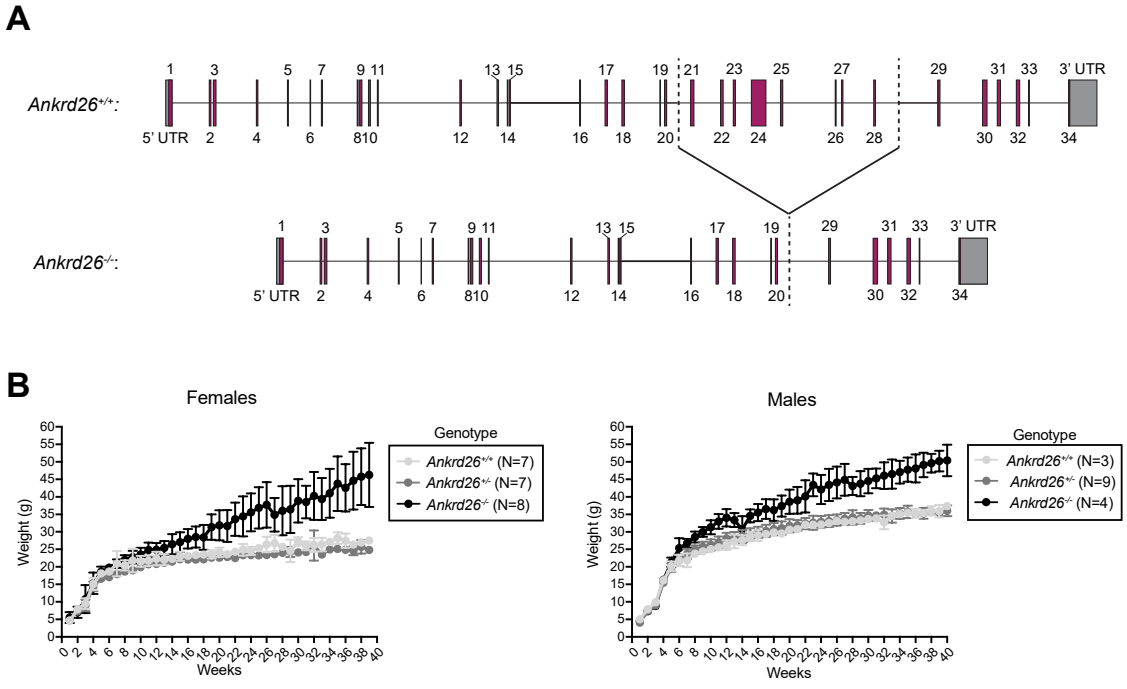

Figure 5.1 A. Schematic of the mouse Ankrd26 allele and the CRISPR deletion produced in *Ankrd26*$^{-/-}$ mice. B. Weights of female (left) and male (right) mice with the indicated *Ankrd26* genotype. Data were collected across the indicated number of mice for each genotype. Mean ± s.e.m.

Journal Permissions

JOHN WILEY AND SONS LICENSE
TERMS AND CONDITIONS

May 15, 2021

This Agreement between Johns Hopkins School of Medicine -- Lauren Evans ("You") and John Wiley and Sons ("John Wiley and Sons") consists of your license details and the terms and conditions provided by John Wiley and Sons and Copyright Clearance Center.

License Number	5070370729744
License date	May 15, 2021
Licensed Content Publisher	John Wiley and Sons
Licensed Content Publication	The EMBO Journal
Licensed Content Title	ANKRD26 recruits PIDD1 to centriolar distal appendages to activate the PIDDosome following centrosome amplification
Licensed Content Author	Lauren T Evans, Taylor Anglen, Phillip Scott, et al
Licensed Content Date	Dec 22, 2020
Licensed Content Volume	40
Licensed Content Issue	4
Licensed Content Pages	18

Type of use	Dissertation/Thesis
Requestor type	Author of this Wiley article
Format	Print and electronic
Portion	Full article
Will you be translating?	No
Title	Centrioles function as signaling centers to control proliferation in cells with centriole amplification
Institution name	Johns Hopkins School of Medicine
Expected presentation date	May 2021
Requestor Location	Johns Hopkins School of Medicine 725 N. Wolfe St. Rm. 704 BALTIMORE, MD 21205 United States Attn: Johns Hopkins School of Medicine
Publisher Tax ID	EU826007151
Total	0.00 USD

Terms and Conditions

TERMS AND CONDITIONS

This copyrighted material is owned by or exclusively licensed to John Wiley & Sons, Inc. or one of its group companies (each a"Wiley Company") or handled on behalf of a society with which a Wiley Company has exclusive publishing rights in relation to a particular work (collectively "WILEY"). By clicking "accept" in connection with completing this licensing transaction, you agree that the following terms and conditions apply to this transaction (along with the billing and payment terms and conditions established by the Copyright Clearance Center Inc., ("CCC's Billing and Payment terms and conditions"), at the time that

you opened your RightsLink account (these are available at any time at http://myaccount.copyright.com).

Terms and Conditions

- The materials you have requested permission to reproduce or reuse (the "Wiley Materials") are protected by copyright.

- You are hereby granted a personal, non-exclusive, non-sub licensable (on a stand-alone basis), non-transferable, worldwide, limited license to reproduce the Wiley Materials for the purpose specified in the licensing process. This license, **and any CONTENT (PDF or image file) purchased as part of your order,** is for a one-time use only and limited to any maximum distribution number specified in the license. The first instance of republication or reuse granted by this license must be completed within two years of the date of the grant of this license (although copies prepared before the end date may be distributed thereafter). The Wiley Materials shall not be used in any other manner or for any other purpose, beyond what is granted in the license. Permission is granted subject to an appropriate acknowledgement given to the author, title of the material/book/journal and the publisher. You shall also duplicate the copyright notice that appears in the Wiley publication in your use of the Wiley Material. Permission is also granted on the understanding that nowhere in the text is a previously published source acknowledged for all or part of this Wiley Material. Any third party content is expressly excluded from this permission.

- With respect to the Wiley Materials, all rights are reserved. Except as expressly granted by the terms of the license, no part of the Wiley Materials may be copied, modified, adapted (except for minor reformatting required by the new Publication), translated, reproduced, transferred or distributed, in any form or by any means, and no derivative works may be made based on the Wiley Materials without the prior permission of the respective copyright owner.**For STM Signatory Publishers clearing permission under the terms of the STM Permissions Guidelines only, the terms of the license are extended to include subsequent editions and for editions in other languages, provided such editions are for the work as a whole in situ and does not involve the separate exploitation of the permitted figures or extracts,** You may not alter, remove or suppress in any manner any copyright, trademark or other notices displayed by the Wiley Materials. You may not license, rent, sell, loan, lease, pledge, offer as security, transfer or assign the Wiley Materials on a stand-alone basis, or any of the rights granted to you hereunder to any other person.

- The Wiley Materials and all of the intellectual property rights therein shall at all times remain the exclusive property of John Wiley & Sons Inc, the Wiley Companies, or their respective licensors, and your interest therein is only that of having possession of and the right to reproduce the Wiley Materials pursuant to Section 2 herein during the continuance of this Agreement. You agree that you own no right, title or interest in or to the Wiley Materials or any of the intellectual property rights therein. You shall have no rights hereunder other than the license as provided for above in Section 2. No right, license or interest to any trademark, trade name, service mark or other branding ("Marks") of WILEY or its licensors is granted hereunder, and you agree that you shall not assert any such right, license or interest with respect thereto

- NEITHER WILEY NOR ITS LICENSORS MAKES ANY WARRANTY OR REPRESENTATION OF ANY KIND TO YOU OR ANY THIRD PARTY, EXPRESS, IMPLIED OR STATUTORY, WITH RESPECT TO THE MATERIALS

OR THE ACCURACY OF ANY INFORMATION CONTAINED IN THE MATERIALS, INCLUDING, WITHOUT LIMITATION, ANY IMPLIED WARRANTY OF MERCHANTABILITY, ACCURACY, SATISFACTORY QUALITY, FITNESS FOR A PARTICULAR PURPOSE, USABILITY, INTEGRATION OR NON-INFRINGEMENT AND ALL SUCH WARRANTIES ARE HEREBY EXCLUDED BY WILEY AND ITS LICENSORS AND WAIVED BY YOU.

- WILEY shall have the right to terminate this Agreement immediately upon breach of this Agreement by you.
- You shall indemnify, defend and hold harmless WILEY, its Licensors and their respective directors, officers, agents and employees, from and against any actual or threatened claims, demands, causes of action or proceedings arising from any breach of this Agreement by you.
- IN NO EVENT SHALL WILEY OR ITS LICENSORS BE LIABLE TO YOU OR ANY OTHER PARTY OR ANY OTHER PERSON OR ENTITY FOR ANY SPECIAL, CONSEQUENTIAL, INCIDENTAL, INDIRECT, EXEMPLARY OR PUNITIVE DAMAGES, HOWEVER CAUSED, ARISING OUT OF OR IN CONNECTION WITH THE DOWNLOADING, PROVISIONING, VIEWING OR USE OF THE MATERIALS REGARDLESS OF THE FORM OF ACTION, WHETHER FOR BREACH OF CONTRACT, BREACH OF WARRANTY, TORT, NEGLIGENCE, INFRINGEMENT OR OTHERWISE (INCLUDING, WITHOUT LIMITATION, DAMAGES BASED ON LOSS OF PROFITS, DATA, FILES, USE, BUSINESS OPPORTUNITY OR CLAIMS OF THIRD PARTIES), AND WHETHER OR NOT THE PARTY HAS BEEN ADVISED OF THE POSSIBILITY OF SUCH DAMAGES. THIS LIMITATION SHALL APPLY NOTWITHSTANDING ANY FAILURE OF ESSENTIAL PURPOSE OF ANY LIMITED REMEDY PROVIDED HEREIN.
- Should any provision of this Agreement be held by a court of competent jurisdiction to be illegal, invalid, or unenforceable, that provision shall be deemed amended to achieve as nearly as possible the same economic effect as the original provision, and the legality, validity and enforceability of the remaining provisions of this Agreement shall not be affected or impaired thereby.
- The failure of either party to enforce any term or condition of this Agreement shall not constitute a waiver of either party's right to enforce each and every term and condition of this Agreement. No breach under this agreement shall be deemed waived or excused by either party unless such waiver or consent is in writing signed by the party granting such waiver or consent. The waiver by or consent of a party to a breach of any provision of this Agreement shall not operate or be construed as a waiver of or consent to any other or subsequent breach by such other party.
- This Agreement may not be assigned (including by operation of law or otherwise) by you without WILEY's prior written consent.
- Any fee required for this permission shall be non-refundable after thirty (30) days from receipt by the CCC.
- These terms and conditions together with CCC's Billing and Payment terms and conditions (which are incorporated herein) form the entire agreement between you and WILEY concerning this licensing transaction and (in the absence of fraud) supersedes

all prior agreements and representations of the parties, oral or written. This Agreement may not be amended except in writing signed by both parties. This Agreement shall be binding upon and inure to the benefit of the parties' successors, legal representatives, and authorized assigns.

- In the event of any conflict between your obligations established by these terms and conditions and those established by CCC's Billing and Payment terms and conditions, these terms and conditions shall prevail.
- WILEY expressly reserves all rights not specifically granted in the combination of (i) the license details provided by you and accepted in the course of this licensing transaction, (ii) these terms and conditions and (iii) CCC's Billing and Payment terms and conditions.
- This Agreement will be void if the Type of Use, Format, Circulation, or Requestor Type was misrepresented during the licensing process.
- This Agreement shall be governed by and construed in accordance with the laws of the State of New York, USA, without regards to such state's conflict of law rules. Any legal action, suit or proceeding arising out of or relating to these Terms and Conditions or the breach thereof shall be instituted in a court of competent jurisdiction in New York County in the State of New York in the United States of America and each party hereby consents and submits to the personal jurisdiction of such court, waives any objection to venue in such court and consents to service of process by registered or certified mail, return receipt requested, at the last known address of such party.

WILEY OPEN ACCESS TERMS AND CONDITIONS

Wiley Publishes Open Access Articles in fully Open Access Journals and in Subscription journals offering Online Open. Although most of the fully Open Access journals publish open access articles under the terms of the Creative Commons Attribution (CC BY) License only, the subscription journals and a few of the Open Access Journals offer a choice of Creative Commons Licenses. The license type is clearly identified on the article.

The Creative Commons Attribution License

The Creative Commons Attribution License (CC-BY) allows users to copy, distribute and transmit an article, adapt the article and make commercial use of the article. The CC-BY license permits commercial and non-

Creative Commons Attribution Non-Commercial License

The Creative Commons Attribution Non-Commercial (CC-BY-NC)License permits use, distribution and reproduction in any medium, provided the original work is properly cited and is not used for commercial purposes.(see below)

Creative Commons Attribution-Non-Commercial-NoDerivs License

The Creative Commons Attribution Non-Commercial-NoDerivs License (CC-BY-NC-ND) permits use, distribution and reproduction in any medium, provided the original work is properly cited, is not used for commercial purposes and no modifications or adaptations are made. (see below)

Use by commercial "for-profit" organizations

Use of Wiley Open Access articles for commercial, promotional, or marketing purposes requires further explicit permission from Wiley and will be subject to a fee.

Further details can be found on Wiley Online Library
http://olabout.wiley.com/WileyCDA/Section/id-410895.html

Other Terms and Conditions:

v1.10 Last updated September 2015

Questions? customercare@copyright.com or +1-855-239-3415 (toll free in the US) or +1-978-646-2777.

Curriculum vitae

Lauren Evans

Johns Hopkins School of Medicine
Holland Lab, Department of Molecular Biology and Genetics
725 N. Wolfe St. Baltimore, MD 21201
(716)-471-2809
levans38@jhmi.edu

Professional Summary

Molecular biologist with experience designing and executing experiments *in vitro* and *in vivo* to study cell growth and **tumorigenesis**

- Expertise in a variety of laboratory techniques, including isolation and cloning of DNA, use of **CRISPR/Cas9 technology** to manipulate cultured cells and generation of mouse models to study tumor initiation and progression
- Proficient at **scientific communication** and mentorship: served as a teaching assistant, molecular biology tutor, mentored several undergraduate students and presented research at several conferences
- Acquired experience in **diverse fields of study**, including biochemistry, immunology and molecular/cell biology

Education

Johns Hopkins University School of Medicine, Baltimore MD August 2016-present

PhD, Human Genetics and Molecular Biology
Thesis: Determining how cells sense and respond to centriole amplification

Canisius College, Buffalo NY August 2012-May 2016

B.S., Biochemistry ACS certified

Research Experience

Graduate Student, Johns Hopkins University School of Medicine 2016-present

Department of Molecular Biology and Genetics
Advisor: Andrew Holland, PhD

- Analyzed the role of centriole amplification in cell growth and tumorigenesis both *in vitro* and *in vivo*
- Utilized a CRISPR/Cas9 genome-wide screen to discover a novel regulator of the centriole amplification response
- Developed a KO mouse model for this novel regulator to study its role in tumor initiation and progression

This work resulted in a first-author as well as two contributing author publications and was funded by the NSF Graduate Research Fellowship Program fellowship

Discovery Research Intern, NextCure October 2020-January 2021

Advisor: Shashank Patel, PhD

- Validated receptor binding of a potential target for immune therapeutics
- Developed a novel validation pipeline for CRISPR screening

Undergraduate Researcher, Roswell Park Cancer Center 2014-2016

Department of Immunology
Advisor: Elizabeth Repasky, PhD

- Developed *in vitro* and *in vivo* systems to investigate the role of β-adrenergic signaling in the response of tumor cells to chemotherapy and radiation
- Discovered adrenergic signaling enhances tumor cell survival by suppressing T-cell-mediated anti-tumor immunity

This work resulted in two contributing author publications

Undergraduate Researcher, Canisius College May 2013-May 2016

Department of Chemistry and Biochemistry
Advisor: Sarah Evans, PhD

- Studied the DNA binding properties of the BosR transcription factor of *B.burgdorferi* (the causative agent of Lyme disease)
- Identified a single amino acid that was critical for the sequence-specific DNA binding of BosR
- Examined metal cofactors that act to competitively inhibit the interaction of BosR with DNA

Skills and Techniques

Lab techniques:

- DNA and RNA extraction from cultured mammalian cells

- Analysis of proteins using **immunoblot**, flow cytometry, co-immunoprecipitation and immunofluorescence microscopy
- Manipulation of **cultured mammalian cells** including generation of gene overexpression, gene knock-out and endogenously tagged cell lines
- Designing and generating DNA constructs through **molecular cloning**
- **Lentiviral production** and cell transduction to generate stable cell lines
- Experience with mouse techniques including breeding, genotyping, bone-marrow extraction/replacement and isolation of blood cells from the submandibular vein

Software:
Microsoft Word/Excel/Powerpoint, Endnote, SnapGene, Adobe Illustrator, Fiji (ImageJ), GraphPad Prism, FlowJo, Leica Application Suite X

Select Fellowships and Awards

Michael DiMaio, M.D. Research Prize 2021

Presented annually to graduate students in the Molecular Biology and Genetics department at JHSOM for the quality, originality and significance of their thesis work

NSF Graduate Research Fellowship Program 2018-present

Presented to graduate students who demonstrate potential for significant research achievement

WNY ACS Student General Excellence Award in Biochemistry 2016

Awarded annually to a student who demonstrates outstanding academic achievement and a strong commitment to service within their community

Publications

In Print:

Evans, L.T., Anglen, T., Scott, P., Lukasik, K., Loncarek, J., Holland, A. J. (2020) ANKRD26 recruits PIDD1 to distal appendages to activate the PIDDosome following centrosome amplification. *EMBO J*

Yeow, Z.Y.*, Lambrus, B.G.*, Marlow, R., Zhan, K.H., Durin, M., **Evans, L.T.**, Scott, P.M., Phan, T., Park, E., Ruiz, L.A., Moralli, D., Knight, E.G., Badder, L.M., Novo, D., Haider, S., Green, C.M., Turr, A.N.J., Lord, C.J., Chapman, J.R.* and Holland, A.J.* (202) Targeting TRIM37-driven centrosome dysfunction in 17q23-amplified breast cancer. *Nature*

MacDonald, C. R., Bucsek, M. J., Qiao, G., Chem, M., **Evans, L.**, Greenberg, D., J., Uccello, T. P., Battaglia, N. G., Hylander, B. L., Singh,

A. K., Lord, E. M., Gerber, S. A., Repasky, E. A. (2019) Adrenergic Receptor Signaling Regulates the Response of Tumors to Ionizing Radiation. *Radiat Res.*

Bowler, M., Kong, D., Sun, S., Nanjundappa, R., **Evans, L.**, Farmer, V., Holland, A. J., Mahjoub, M. R., Sui, H., Loncarek, J. (2019) High-resolution characterization of centriole distal appendage morphology and dynamics by correlative STORM and electron microscopy. *Nat Commun.*

Evans, L.T., Holland, A.J. (2018) Pushed out of a tough crowd: centrosome aberrations promote invasiveness. *EMBO J.*

Bucsek, M. J., Qiao, G., MacDonald, C. R., Giridharan, T., **Evans, L.**, Niedzwecki, B., Liu, H., Kokolus, K. M., Eng, J. W-L., Messmer, M. N., Attwood, K., Abrams, S. I., Hylander, B. L., Repasky, E. A. (2017) β-Adrenergic Signaling in Mice Housed at Standard Temperatures Suppresses an Effector Phenotype in CD8 + T Cells and Undermines Checkpoint Inhibitor Therapy. *Cancer Res.*

Select Presentations

Oral Presentations:

Evans, L., Anglen, T. Loncarek, J., Holland, AJ. (2019) Determining the role of the PIDDosome in the centriole amplification response. Centrosome Meeting, Fredrick, MD.

Poster Presentations:

Evans, L., Anglen, T., Holland, AJ. (2019) CRISPR/Cas9 genome-wide knock-out screen to identify novel regulators of the centriole amplification response. EMBO Chromosome Missegregation and Aneuploidy workshop, Cascais, Portugal.

Evans, L., Anglen, T., Holland, AJ. (2018) CRISPR/Cas9 genome-wide knock-out screen to identify novel regulators of the centriole amplification response. The Mid-Atlantic Mitosis and Meiosis Meeting, Baltimore, MD.

Evans, L., Anglen, T., Holland, AJ. (2017) Using genome wide CRISPR/ Cas9 screens to elucidate how cells arrest following centrosome amplification. ASCB/EMBO Meeting, Philadelphia, PA.

References

1. Nigg, E. A. & Holland, A. J. Once and only once: Mechanisms of centriole duplication and their deregulation in diseases. *Nature Reviews Molecular Cell Biology* vol. 19 297–312 (2018).
2. Gönczy, P. Towards a molecular architecture of centriole assembly. *Nature Reviews Molecular Cell Biology* vol. 13 425–435 (2012).
3. Firat-Karalar, E. N. & Stearns, T. The centriole duplication cycle. *Philosophical Transactions of the Royal Society B: Biological Sciences* vol. 369 (2014).
4. Hatch, E. & Stearns, T. The life cycle of centrioles. *Cold Spring Harb. Symp. Quant. Biol.* **75**, 425–431 (2010).
5. Tanos, B. E. *et al.* Centriole distal appendages promote membrane docking, leading to cilia initiation. *Genes Dev.* **27**, 163–168 (2013).
6. Nigg, E. A. & Stearns, T. The centrosome cycle: Centriole biogenesis, duplication and inherent asymmetries. *Nature Cell Biology* vol. 13 1154–1160 (2011).
7. Chan, J. Y. A clinical overview of centrosome amplification in human cancers. *International Journal of Biological Sciences* vol. 7 1122–1144 (2011).
8. Wang, M., Nagle, R. B., Knudsen, B. S., Cress, A. E. & Rogers, G. C. Centrosome loss results in an unstable genome and malignant prostate tumors. *Oncogene* **39**, 399–413 (2020).
9. Azimzadeh, J., Wong, M. L., Downhour, D. M., Alvarado, A. S. & Marshall, W. F. Centrosome loss in the evolution of planarians. *Science (80-.).* **335**, 461–463 (2012).
10. Debec, A., Sullivan, W. & Bettencourt-Dias, M. Centrioles: Active players or passengers during mitosis? *Cellular and Molecular Life Sciences* vol. 67 2173–2194 (2010).
11. Prosser, S. L. & Pelletier, L. Mitotic spindle assembly in animal cells: A fine balancing act. *Nature Reviews Molecular Cell Biology* vol. 18 187–201 (2017).
12. Bazzi, H. & Anderson, K. V. Acentriolar mitosis activates a p53-dependent apoptosis pathway in the mouse embryo. *Proc. Natl. Acad. Sci. U. S. A.* **111**, (2014).
13. Hayward, D., Metz, J., Pellacani, C. & Wakefield, J. G. Synergy between Multiple Microtubule-Generating Pathways Confers Robustness to Centrosome-Driven Mitotic Spindle Formation. *Dev. Cell* **28**, 81–93 (2014).
14. Goshima, G., Mayer, M., Zhang, N., Stuurman, N. & Vale, R. D. Augmin: A protein complex required for centrosome-independent microtubule generation within the spindle. *J. Cell Biol.* **181**, 421–429 (2008).
15. Lambrus, B. G. *et al.* A USP28-53BP1-p53-p21 signaling axis arrests growth after centrosome loss or prolonged mitosis. *J. Cell Biol.* **214**, 143–153 (2016).
16. Meitinger, F. *et al.* 53BP1 and USP28 mediate p53 activation and G1

arrest after centrosome loss or extended mitotic duration. *J. Cell Biol.* **214**, 155–166 (2016).
17. Fong, C. S. *et al.* 53BP1 and USP28 mediate p53- dependent cell cycle arrest in response to centrosome loss and prolonged mitosis. *Elife* **5**, (2016).
18. Zimmermann, M. & De Lange, T. 53BP1: Pro choice in DNA repair. *Trends in Cell Biology* vol. 24 108–117 (2014).
19. Knobel, P. A. *et al.* USP28 Is Recruited to Sites of DNA Damage by the Tandem BRCT Domains of 53BP1 but Plays a Minor Role in Double-Strand Break Metabolism. *Mol. Cell. Biol.* **34**, 2062–2074 (2014).
20. Ganem, N. J., Godinho, S. A. & Pellman, D. A mechanism linking extra centrosomes to chromosomal instability. *Nature* **460**, 278–282 (2009).
21. Godinho, S. A. *et al.* Oncogene-like induction of cellular invasion from centrosome amplification. *Nature* **510**, 167–171 (2014).
22. LoMastro, G. M. & Holland, A. J. The Emerging Link between Centrosome Aberrations and Metastasis. *Developmental Cell* vol. 49 325–331 (2019).
23. Coelho, P. A. *et al.* Over-expression of Plk4 induces centrosome amplification, loss of primary cilia and associated tissue hyperplasia in the mouse. *Open Biol.* **5**, (2015).
24. Levine, M. S. *et al.* Centrosome Amplification Is Sufficient to Promote Spontaneous Tumorigenesis in Mammals. *Dev. Cell* **40**, 313-322.e5 (2017).
25. Basto, R. *et al.* Centrosome Amplification Can Initiate Tumorigenesis in Flies. *Cell* **133**, 1032–1042 (2008).
26. Serçin, Ö. *et al.* Transient PLK4 overexpression accelerates tumorigenesis in p53-deficient epidermis. *Nat. Cell Biol.* **18**, 100–110 (2016).
27. Galofré, C. *et al.* Centrosome reduction in newly-generated tetraploid cancer cells obtained by separase depletion. *Sci. Rep.* **10**, 1–12 (2020).
28. Fujiwara, T. *et al.* Cytokinesis failure generating tetraploids promotes tumorigenesis in p53-null cells. *Nature* **437**, 1043–1047 (2005).
29. Bielski, C. M. *et al.* Genome doubling shapes the evolution and prognosis of advanced cancers. *Nat. Genet.* **50**, 1189–1195 (2018).
30. Fava, L. L. *et al.* The PIDDosome activates p53 in response to supernumerary centrosomes. *Genes Dev.* **31**, 34–45 (2017).
31. Holland, A. J. *et al.* The autoregulated instability of Polo-like kinase 4 limits centrosome duplication to once per cell cycle. *Genes Dev.* **26**, 2684–2689 (2012).
32. Ganem, N. J. *et al.* Cytokinesis failure triggers hippo tumor suppressor pathway activation. *Cell* **158**, 833–848 (2014).
33. Bolgioni, A. F. & Ganem, N. J. The interplay between centrosomes and the Hippo tumor suppressor pathway. *Chromosome Research* vol. 24 93–104 (2016).
34. Pan, D. The hippo signaling pathway in development and cancer. *Developmental Cell* vol. 19 491–505 (2010).
35. Tinel, A. & Tschopp, J. The PIDDosome, a Protein Complex Implicated in Activation of Caspase-2 in Response to Genotoxic Stress. *Science (80-.).*

304, 843–846 (2004).
36. Sladky, V., Schuler, F., Fava, L. L. & Villunger, A. The resurrection of the PIDDosome - Emerging roles in the DNA-damage response and centrosome surveillance. *Journal of Cell Science* vol. 130 3779–3787 (2017).
37. Ganem, N. J. & Pellman, D. Linking abnormal mitosis to the acquisition of DNA damage. *Journal of Cell Biology* vol. 199 871–881 (2012).
38. Chen, S. *et al.* Genome-wide CRISPR screen in a mouse model of tumor growth and metastasis. *Cell* **160**, 1246–1260 (2015).
39. Shalem, O. *et al.* Genome-scale CRISPR-Cas9 knockout screening in human cells. *Science (80-.).* **343**, 84–87 (2014).
40. Langmead, B., Trapnell, C., Pop, M. & Salzberg, S. L. Ultrafast and memory-efficient alignment of short DNA sequences to the human genome. *Genome Biol.* **10**, (2009).
41. Li, W. *et al.* MAGeCK enables robust identification of essential genes from genome-scale CRISPR/Cas9 knockout screens. *Genome Biol.* **15**, 554 (2014).
42. Cerami, E. *et al.* The cBio Cancer Genomics Portal: An open platform for exploring multidimensional cancer genomics data. *Cancer Discov.* **2**, 401–404 (2012).
43. Yabuta, N. *et al.* Lats2 is an essential mitotic regulator required for the coordination of cell division. *J. Biol. Chem.* **282**, 19259–19271 (2007).
44. Evans, L. T. *et al.* ANKRD26 recruits PIDD1 to centriolar distal appendages to activate the PIDDosome following centrosome amplification. *EMBO J.* **40**, e105106 (2021).
45. Burigotto, M. *et al.* Centriolar distal appendages activate the centrosome-PIDDosome-p53 signalling axis via ANKRD26. *EMBO J.* **40**, e104844 (2021).
46. Reiter, J. F., Blacque, O. E. & Leroux, M. R. The base of the cilium: Roles for transition fibres and the transition zone in ciliary formation, maintenance and compartmentalization. *EMBO Reports* vol. 13 608–618 (2012).
47. Fliegauf, M., Benzing, T. & Omran, H. When cilia go bad: Cilia defects and ciliopathies. *Nature Reviews Molecular Cell Biology* vol. 8 880–893 (2007).
48. Ishikawa, H., Kubo, A., Tsukita, S. & Tsukita, S. Odf2-deficient mother centrioles lack distal/subdistal appendages and the ability to generate primary cilia. *Nat. Cell Biol.* **7**, 517–524 (2005).
49. Bowler, M. *et al.* High-resolution characterization of centriole distal appendage morphology and dynamics by correlative STORM and electron microscopy. *Nat. Commun.* **10**, (2019).
50. Ye, X., Zeng, H., Ning, G., Reiter, J. F. & Liu, A. C2cd3 is critical for centriolar distal appendage assembly and ciliary vesicle docking in mammals. *Proc. Natl. Acad. Sci. U. S. A.* **111**, 2164–2169 (2014).
51. Yang, T. T. *et al.* Super-resolution architecture of mammalian centriole distal appendages reveals distinct blade and matrix functional components. *Nat. Commun.* **9**, (2018).
52. Park, H. H. *et al.* Death Domain Assembly Mechanism Revealed by Crystal

Structure of the Oligomeric PIDDosome Core Complex. *Cell* **128**, 533–546 (2007).
53. Bluteau, D. *et al.* Thrombocytopenia-associated mutations in the ANKRD26 regulatory region induce MAPK hyperactivation. *J. Clin. Invest.* **124**, 580–591 (2014).
54. Marconi, C. *et al.* 5′UTR point substitutions and N-terminal truncating mutations of ANKRD26 in acute myeloid leukemia. *J. Hematol. Oncol.* **10**, (2017).
55. Bera, T. K. *et al.* A model for obesity and gigantism due to disruption of the Ankrd26 gene. *Proc. Natl. Acad. Sci. U. S. A.* **105**, 270–275 (2008).
56. Acs, P. *et al.* A novel form of ciliopathy underlies hyperphagia and obesity in Ankrd26 knockout mice. *Brain Struct. Funct.* **220**, 1511–1528 (2015).
57. Moyer, T. C., Clutario, K. M., Lambrus, B. G., Daggubati, V. & Holland, A. J. Binding of STIL to Plk4 activates kinase activity to promote centriole assembly. *J. Cell Biol.* **209**, 863–878 (2015).
58. Rothbauer, U. *et al.* A versatile nanotrap for biochemical and functional studies with fluorescent fusion proteins. *Mol. Cell. Proteomics* **7**, 282–289 (2008).
59. Moyer, T. C. & Holland, A. J. Plk4 promotes centriole duplication by phosphorylating stil to link the procentriole cartwheel to the microtubule wall. *Elife* **8**, (2019).
60. Sedjaï, F. *et al.* Control of ciliogenesis by FOR20, a novel centrosome and pericentriolar satellite protein. *J. Cell Sci.* **123**, 2391–2401 (2010).
61. Rebacz, B. *et al.* Identification of griseofulvin as an inhibitor of centrosomal clustering in a phenotype-based screen. *Cancer Res.* **67**, 6342–6350 (2007).
62. Sladky, V. C. & Villunger, A. Uncovering the PIDDosome and caspase-2 as regulators of organogenesis and cellular differentiation. *Cell Death and Differentiation* vol. 27 2037–2047 (2020).
63. Tinel, A. *et al.* Autoproteolysis of PIDD marks the bifurcation between pro-death caspase-2 and pro-survival NF-κB pathway. *EMBO J.* **26**, 197–208 (2007).
64. Wang, R. *et al.* Autoinhibition of UNC5b Revealed by the Cytoplasmic Domain Structure of the Receptor. *Mol. Cell* **33**, 692–703 (2009).
65. Pippucci, T. *et al.* Mutations in the 5′ UTR of ANKRD26, the ankirin repeat domain 26 gene, cause an autosomal-dominant form of inherited thrombocytopenia, THC2. *Am. J. Hum. Genet.* **88**, 115–120 (2011).
66. Noris, P. *et al.* Mutations in ANKRD26 are responsible for a frequent form of inherited thrombocytopenia: Analysis of 78 patients from 21 families. *Blood* **117**, 6673–6680 (2011).
67. Falcieri, E. *et al.* Ultrastructural characterization of maturation, platelet release, and senescence of human cultured megakaryocytes. *Anat. Rec.* **258**, 90–99 (2000).
68. Marquez, R. *et al.* A new family with a germline ANKRD26 mutation and predisposition to myeloid malignancies. *Leukemia and Lymphoma* vol. 55 2945–2946 (2014).

69. Concordet, J. P. & Haeussler, M. CRISPOR: Intuitive guide selection for CRISPR/Cas9 genome editing experiments and screens. *Nucleic Acids Res.* **46**, W242–W245 (2018).
70. Sladky, V. C. *et al.* E2F-Family Members Engage the PIDDosome to Limit Hepatocyte Ploidy in Liver Development and Regeneration. *Dev. Cell* **52**, 335-349.e7 (2020).
71. Wang, M. J., Chen, F., Lau, J. T. Y. & Hu, Y. P. Hepatocyte polyploidization and its association with pathophysiological processes. *Cell death & disease* vol. 8 e2805 (2017).